Bioorg. Med. Chem. 44 (2021) 116292

Contents lists available at ScienceDirect

Bioorganic & Medicinal Chemistry

journal homepage: www.elsevier.com/locate/bmc

Inhibitory activities of anthraquinone and xanthone derivatives against transthyretin amyloidogenesis

Ryota Kitakami [a], Kishin Inui [b], Yusuke Nakagawa [b], Yurika Sawai [c], Wakana Katayama [d], Takeshi Yokoyama [d], Takuya Okada [c,e], Kayoko Kanamitsu [f], Shinsaku Nakagawa [g], Naoki Toyooka [c,e], Mineyuki Mizuguchi [d,*]

[a] Graduate School of Medicine and Pharmaceutical Sciences, University of Toyama, Toyama 930-0194, Japan
[b] Graduate School of Science and Engineering, University of Toyama, Toyama 930-8555, Japan
[c] Faculty of Engineering, University of Toyama, Toyama 930-8555, Japan
[d] Faculty of Pharmaceutical Sciences, University of Toyama, Toyama 930-0914, Japan
[e] Graduate School of Innovative Life Science, University of Toyama, Toyama 930-8555, Japan
[f] Drug Discovery Initiative, the University of Tokyo, Tokyo 113-0033, Japan
[g] Graduate School of Pharmaceutical Sciences, Osaka University, Osaka 565-0871, Japan

ARTICLE INFO

Keywords:
Transthyretin
Stabilizer
X-ray crystallography
Anthraquinone
Xanthone

ABSTRACT

Transthyretin is a tetrameric protein which functions as a transporter of thyroxine and retinol-binding protein. Misfolding and amyloid aggregation of transthyretin are known to cause wild-type and hereditary transthyretin amyloidosis. Stabilization of the transthyretin tetramer by low molecular weight compounds is an efficacious strategy to inhibit the aggregation pathway in the amyloidosis. Here, we investigated the inhibitory activities of anthraquinone and xanthone derivatives against amyloid aggregation, and found that xanthone-2-carboxylic acid with one chlorine or methyl group has strong inhibitory activity comparable with that of diflunisal, which is one of the best known stabilizers of transthyretin. X-ray crystallographic structures of transthyretin in complex with the compounds revealed that the introduction of chlorine, which is buried in a hydrophobic region, is important for the strong inhibitory effect of the stabilizer against amyloidogenesis. An *in vitro* absorption, distribution, metabolism and elimination (ADME) study and *in vivo* pharmacokinetic study demonstrated that the compounds have drug-like features, suggesting that they have potential as therapeutic agents to stabilize transthyretin.

1. Introduction

Amyloidosis is a group of diseases which are caused by deposition of abnormal protein aggregates known as amyloid fibrils in tissues or organs. Amyloid fibrils are built up from amyloidogenic precursor proteins and more than 30 amyloidogenic proteins are currently known.[1]

Transthyretin (TTR), previously called prealbumin, is one of the amyloidogenic proteins. TTR forms a homotetramer with a molecular weight of 55 kDa under physiological conditions and its subunit monomer is composed of 127 amino acid residues. TTR is a serum protein mainly synthesized in the liver, but it is also produced in the choroid plexus of the brain, the pigmented epithelium of the retina, and the islets of Langerhans. TTR circulates in serum at a concentration of 3.1–7.6 μM, and plays a role in transporting thyroid hormone thyroxine (T4) and retinol-loaded retinol-binding protein.[2–5]

TTR does not form amyloid fibrils when the tetramer in the native state is maintained. However, TTR aggregates into amyloid fibrils when it is destabilized due to amyloidogenic amino acid mutations and/or *in vitro* under acidic conditions. Wild-type TTR also possesses an inherent amyloidogenic potential, which causes wild-type TTR amyloidosis, a condition previously called senile systemic amyloidosis.[6] In the amyloid fibril formation of TTR, the tetramer dissociation occurs first, then the monomer unfolds into an amyloidogenic intermediate, which self-aggregates to form amyloid fibrils. The tetramer dissociation is a rate-limiting step of the amyloid fibril formation of TTR.[3,4] So far, more than 130 mutations of TTR that cause hereditary TTR amyloidosis have been reported. Among them, V30M is the best studied mutation, since it is the most frequent amyloidogenic mutation worldwide and there are large foci of hereditary V30M-TTR amyloidosis patients in Portugal, Sweden, and Japan.[7,8]

* Corresponding author.
E-mail address: mineyuki@pha.u-toyama.ac.jp (M. Mizuguchi).

https://doi.org/10.1016/j.bmc.2021.116292
Received 14 December 2020; Received in revised form 17 June 2021; Accepted 21 June 2021
Available online 26 June 2021

Liver transplantation is a well-established treatment for hereditary TTR amyloidosis, since it replaces the amyloidogenic TTR variant in serum with wild-type TTR. However, there is a great need for development of a less invasive treatment. One alternative treatment for liver transplantation is the stabilization of the TTR tetramer by small molecules, such as tafamidis and diflunisal. These compounds bind to the two T4-binding channels located at the dimer-dimer interface of TTR. The binding of the compounds stabilizes the TTR tetramer, which results in the inhibition of the tetramer dissociation and the amyloid fibril formation of TTR.[3,4,9,10] Treatment with tafamidis has been shown

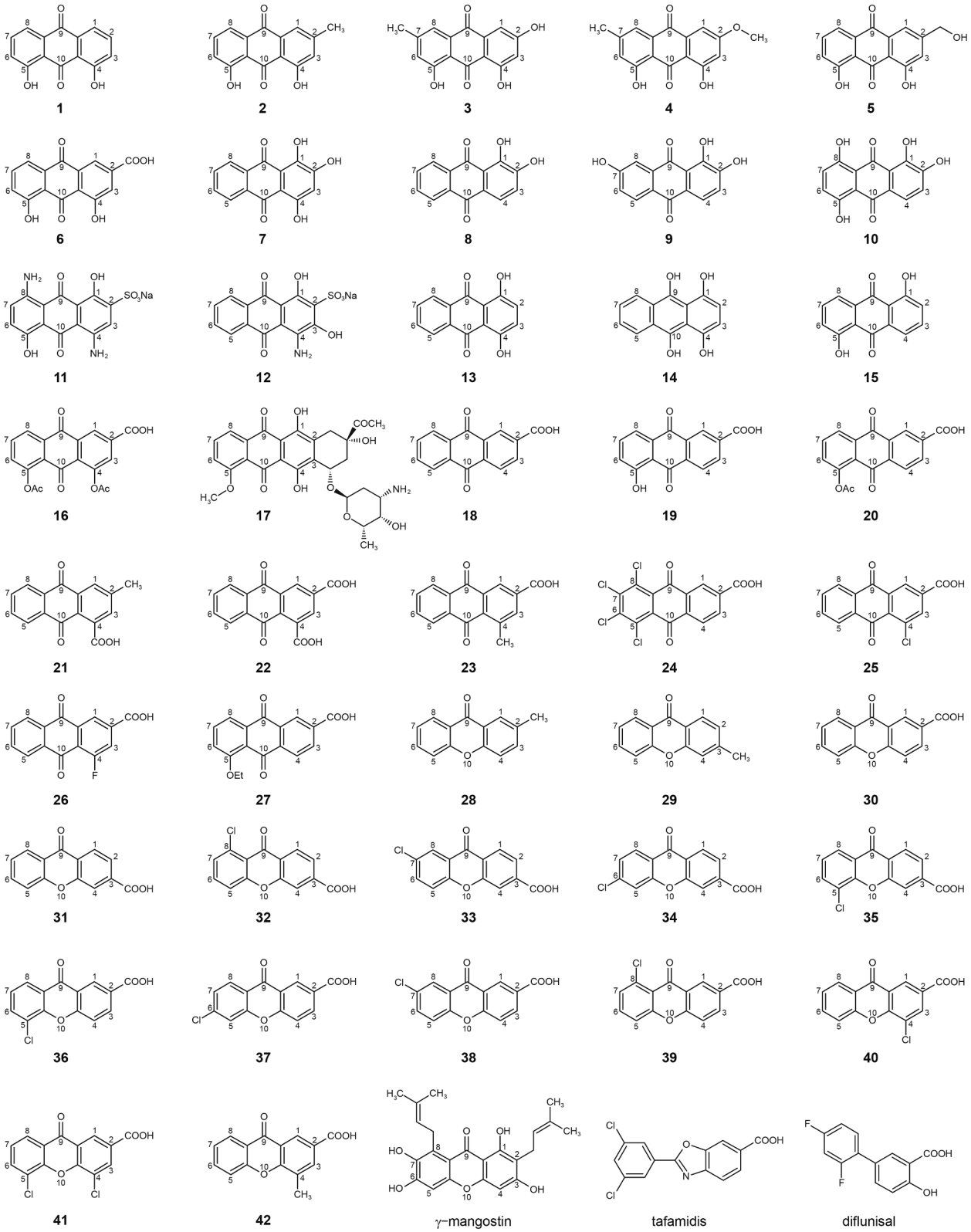

Fig. 1. Chemical structures of anthraquinone derivatives (**1**–**27**), xanthone derivatives (**28**–**42**), and positive controls (tafamidis and diflunisal). The chemical structure of γ-mangostin is also shown for comparison.

to delay the neuropathic progression in patients with familial amyloid polyneuropathy caused by the V30M mutated TTR.[11,12] Tafamidis is the first pharmacotherapy approved for the treatment of neurologic impairment in familial amyloid polyneuropathy. It is also approved for the treatment of cardiomyopathy caused by amyloid deposition of TTR in the heart. Diflunisal has also been shown to reduce the rate of progression of neurological impairment and to preserve quality of life in clinical trials.[13] In addition, tolcapone and AG10 are currently undergoing clinical trials for the treatment of TTR amyloidosis.[14–16]

Liver transplantation and orally administrable TTR kinetic stabilizers (tafamidis and diflunisal) target the native TTR circulating in the blood, which is mainly synthesized in the liver. In addition to the liver, however, smaller amounts of TTR are synthesized in the retina of the eye, the choroid plexus of the brain, and the α cells of the pancreatic islets. In fact, ocular amyloidosis and cerebral amyloid angiopathy accompanied by leptomeningeal amyloidosis are observed in patients with several specific TTR gene mutations.[17–21] Moreover, variant TTR deposition in the eye does not stop after liver transplantation due to TTR biosynthesis in the retinal pigment epithelium.[18,22,23] Central nervous system symptoms due to meningeal and/or cerebrovascular amyloidosis can occur in patients who have survived for a long time after liver transplantation.[22,24] In addition, tafamidis is unable to halt the progression of the disease in patients with advanced polyneuropathy caused by V30M-TTR.[25] Therefore, there is a great need for a new drug for TTR amyloidosis, and the development of such a drug is still being actively pursued.[15,26–30] In order to promote this effort, it may be useful to develop small molecule inhibitors with scaffolds different from tafamidis and diflunisal.

Anthraquinone and xanthone derivatives are a class of tricyclic organic compounds that are present in various natural sources, including plants, bacteria and fungi. Anthraquinone has two keto groups at the central ring, while only one keto group exists in xanthone. These compounds have been widely applied in industry and are expected to be novel therapeutic agents against various diseases such as cancer, infectious diseases, and amyloidosis.[31–38] In a previous study, Baures *et al.* reported that anthraquinone-2-carboxylic acid is modestly effective in inhibiting amyloid aggregation of wild-type TTR.[33] In addition, Maia *et al.* showed that xanthone derivatives isolated from *Calophyllum teysmannii* var. *inophylloide* bind to the T4-binding channels of TTR.[35] We also showed that γ-mangostine, a xanthone derivative found in the pericarp of mangosteen, inhibits the amyloid fibril formation of V30M-TTR *in vitro*.[37] To date, however, there has been no detailed analysis of the relationship between the chemical structure of anthraquinone and xanthone derivatives and their inhibitory activity against amyloid fibril formation. Here, we report detailed comprehensive investigations on the structure–activity relationship of anthraquinone and xanthone derivatives (Fig. 1). We found that xanthone-2-carboxylic acid with a chlorine or methyl group at position 4 has a strong amyloid inhibitory activity comparable with that of the known inhibitor diflunisal (Figure 2). High-resolution crystal structures of TTR in complex with anthraquinone and xanthone derivatives revealed the details of how these compounds bind to the T4-binding channels at the dimer-dimer interface of TTR. In addition, we performed an *in vitro* ADME and *in vivo* pharmacokinetic analysis of the compounds and demonstrated that they have drug-like properties. Our results suggest that these compounds have potential as therapeutic agents to stabilize TTR in the blood.

2. Results and discussion

2.1. Inhibitory activities of anthraquinone derivatives

We examined the inhibitory effect of commercially available anthraquinone derivatives (**1–17**) on the amyloid fibril formation of V30M-TTR. The V30M variant was used in this study, since it is the most frequent amyloidogenic mutation causing hereditary TTR amyloidosis.[7,8] Amyloid fibril formation was initiated by a pH-jump from 7.0 to 4.6 at a tetramer concentration of 10 μM in the presence of 0–100 μM compounds. After incubation for 96 h at 37 °C, the amyloid aggregation was quantified by thioflavin T fluorescence.[37,39,40] Amyloid inhibitory activity was assessed by determining the compound concentration for 50% inhibition of amyloid aggregation (IC_{50}) (Table 1 and

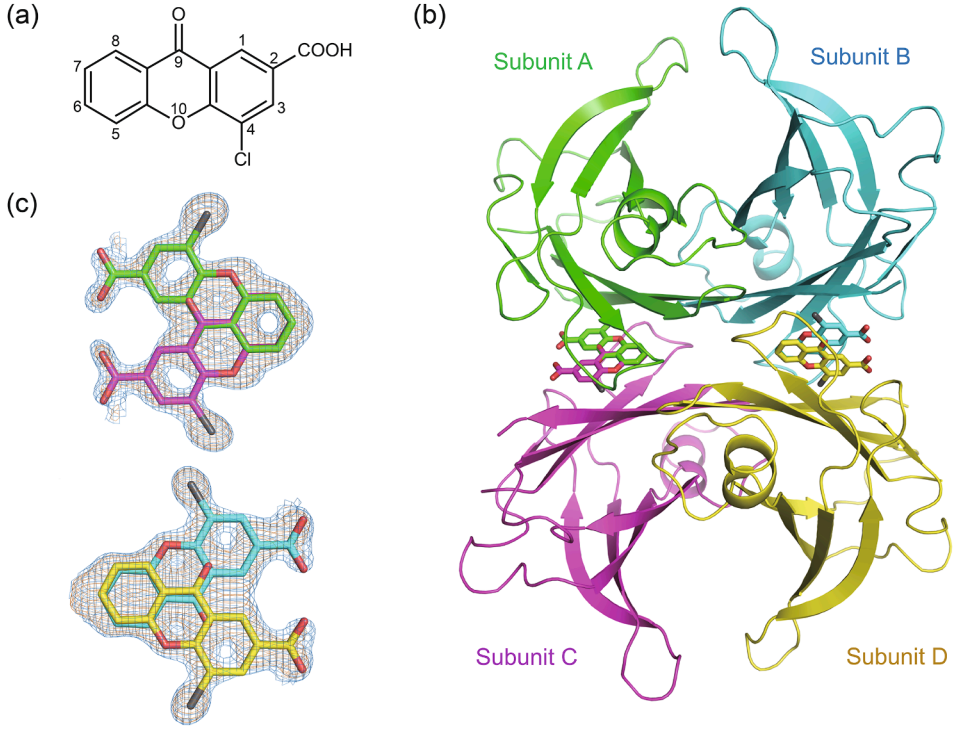

Fig. 2. Structure of compound **40**. (a) Chemical structure of compound **40**. (b) The overall structure of WT-TTR in complex with **40**. (c) Omit difference Fourier map for **40**. Contoured at 3.3 σ (orange mesh) and 2.5 σ (blue mesh).

Table 1
Inhibitory activities of anthraquinone and xanthone derivatives. The IC_{50} values were calculated from the inhibition ratio at 0–100 μM concentration.

Compd No.	IC_{50} (μM)	CLogP
1	>100	3.74
2	>100	4.24
3	>100	3.62
4	>100	4.19
5	>100	2.70
6	12 ± 0.15	3.53
7	12 ± 1.7	3.12
8	>100	3.28
9	12 ± 0.23	2.66
10	>100	2.92
11	>100	0.69
12	11 ± 0.15	0.78
13	>100	3.74
14	>100	2.67
15	>100	3.74
16	5.4 ± 0.28	2.13
17	>100	0.84
18	28 ± 2.6	3.26
19	50 ± 12	3.56
20	10 ± 0.09	2.73
21	45 ± 10	3.76
22	>100	3.04
23	13 ± 0.40	3.76
24	21 ± 2.2	5.76
25	12 ± 0.49	3.99
26	24 ± 1.9	3.76
27	22 ± 1.0	3.83
28	>100	3.48
29	>100	3.48
30	22 ± 0.24	2.85
31	19 ± 0.70	2.85
32	10 ± 0.19	3.57
33	10 ± 0.45	3.57
34	13 ± 0.09	3.57
35	7.7 ± 0.34	3.57
36	13 ± 0.51	3.57
37	>100	3.57
38	12 ± 0.27	3.57
39	13 ± 0.08	3.57
40	6.7 ± 0.26	3.60
41	9.1 ± 0.01	4.31
42	6.5 ± 0.20	3.34
γ-Mangostin	10.0 ± 0.3	5.69
Diflunisal	6.6 ± 0.14	4.39
Tafamidis	5.3 ± 0.60	5.00

Supplementary Fig. 1). Compounds **6**, **7**, **9**, and **12** showed amyloid inhibitory activity with IC_{50} values of 11–12 μM. Compound **16** showed the strongest amyloid inhibitory activity among **1**–**17**, and its IC_{50} value was 5.4 ± 0.28 μM (Fig. 1 and Table 1). Compound **16** is diacerein, which is used to treat the symptoms of osteoarthritis. Diacerein is a prodrug and its active metabolite is rhein (compound **6**). The IC_{50} value of **6** is 12 ± 0.15 μM, and thus its amyloid inhibitory activity is not much weaker than that of diacerein (Fig. 1 and Table 1). However, there is a possibility that the use of diacerein may cause side effects such as diarrhea and hepatobiliary disorders, although it has an acceptable safety profile.[41] Therefore, we explored the possibility of developing other anthraquinone derivatives as potential inhibitors of TTR amyloidosis.

Next, we synthesized the anthraquinone derivatives (**18**–**27**). Syntheses of anthraquinone derivatives **18** and **21**–**26** are shown in Scheme 1.

The anthraquinone skeleton (**A1**–**A5**) was constructed from the appropriate phthalic anhydride and toluene derivative in two steps of Friedel-Crafts reaction followed by the cyclization process.[42] The oxidation of the methyl group on the anthraquinone skeleton with chromium trioxide in an acetic acid (Method A)[43] or with manganese dioxide in a concentrated sulfuric acid (Method B)[44] afforded the

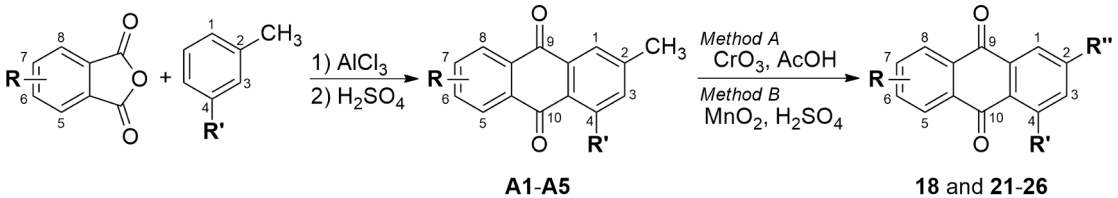

Scheme 1. Syntheses of anthraquinone derivatives **18** and **21**–**26.**

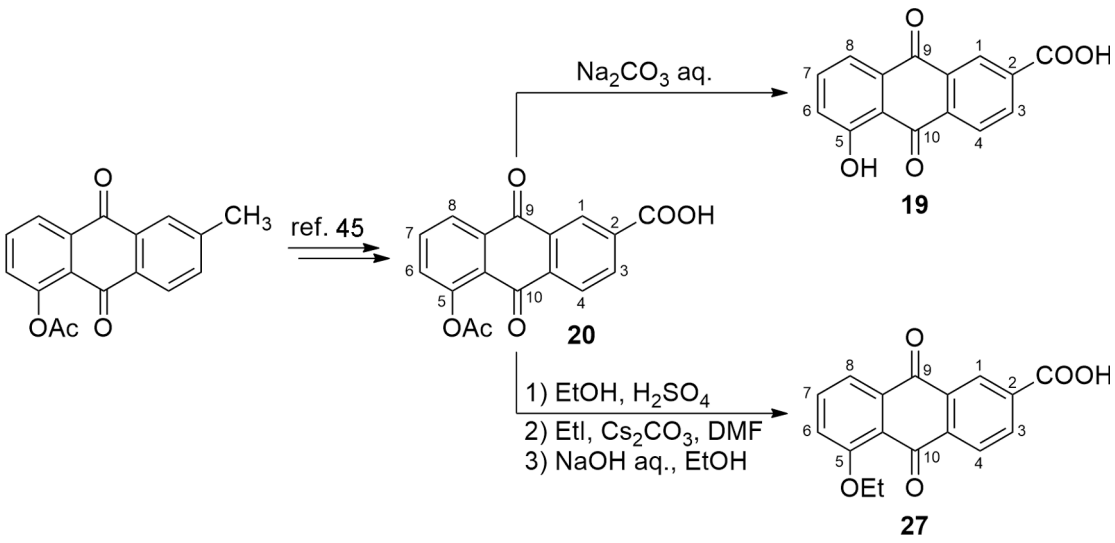

Scheme 2. Syntheses of anthraquinone derivatives **19**–**20** and **27.**

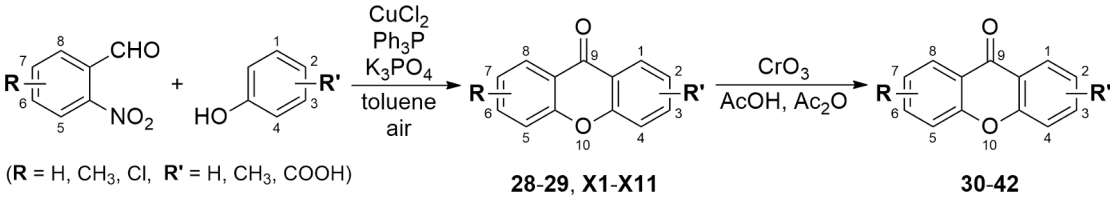

Scheme 3. Syntheses of xanthone derivatives **28**–**42.**

anthraquinone derivatives **18** and **21**–**26**. On the other hand, oxygenated anthraquinone derivatives **19** and **27** were synthesized by the known anthraquinone **20**,[45] which was prepared from 1-acetoxy-6-methylanthraquinone as shown in Scheme 2. The acetyl group of **20** was hydrolyzed with sodium carbonate solution to give the anthraquinone **19**. Moreover, anthraquinone **20** was transformed into the corresponding ethyl ether in two steps, followed by hydrolysis of the resulting ethyl ester with sodium hydroxide to obtain the anthraquinone **27**.

The IC_{50} values of **18**–**27** are summarized in Table 1. A comparison of the IC_{50} values of **16**, **18**, and **20** indicates that acetoxy groups at both the 4 and 5 positions are important for the amyloid inhibitory activity of **16** (Fig. 1 and Table 1). From the IC_{50} values for compounds **18**, **19**, **20**, and **27**, the compound with an acetoxy group at position 5 (**20**) has higher inhibitory activity than the compounds with hydrogen (**18**), hydroxyl (**19**), and ethoxy (**27**) groups at position 5 (Fig. 1 and Table 1).

Anthraquinone-2-carboxylic acid (compound **18**) showed an IC_{50} value of 28 ± 2.6 μM, which was significantly higher than that of the positive controls (diflunisal and tafamidis) (Table 1). This is consistent with a previous study which showed that anthraquinone-2-carboxylic acid is only modestly effective in inhibiting amyloid fibril formation of wild-type TTR *in vitro*.[33] A comparison of **21** and **23** shows that the carboxy group at position 2 is important for the inhibitory activity. Compound **22**, which has carboxy groups at both positions 2 and 4, showed little inhibitory activity (Fig. 1 and Table 1).

2.2. Inhibitory activities of xanthone derivatives

We synthesized the xanthone derivatives (**28**–**42**) and investigated their amyloid inhibitory activity (Fig. 1 and Table 1). Xanthone derivatives **28**–**42** were synthesized from the appropriate *o*-nitrobenzaldehyde and a phenol derivative in the presence of $CuCl_2$, Ph_3P, and K_3PO_4 in toluene at 100 °C, as shown in Scheme 3.[46,47]

Compounds **30** and **31**, in which carboxyl groups are introduced into xanthone, both show IC_{50} values of approximately 20 μM, while compounds **28** and **29**, in which methyl groups are introduced at the same position, do not inhibit amyloid fibril formation (Fig. 1 and Table 1). These results indicate that the carboxy group at position 2 or 3 in xanthone is important for the amyloid inhibitory activity. Compound **40** is an analogue of **25**, and the comparison of their IC_{50} values suggests that the xanthone derivatives have stronger inhibitory activity than the corresponding anthraquinone derivatives (Fig. 1 and Table 1). Similarly, compound **42** is a xanthone derivative of **23**, and its inhibitory activity is higher than that of **23**. Among the xanthone derivatives in this study, **40** and **42**, in which a carboxyl group is introduced at position 2 and a chlorine or a methyl group is introduced at position 4, exhibited the strongest inhibitory activities, which were comparable with that of diflunisal (Fig. 1 and Table 1). We confirmed the binding of **40** and **42** to V30M-TTR using isothermal titration calorimetry (ITC): the binding affinities of **40** and **42** were lower than that of tafamidis, but were comparable with that of diflunisal (Supplementary Fig. 2).

2.3. Binding modes of anthraquinone and xanthone derivatives

To elucidate the detailed binding mechanisms of the anthraquinone and xanthone derivatives, we determined the crystal structures of TTR (wild-type and/or V30M) in complex with **7**, **25**, **32** and **40** at 1.15–1.45 Å resolutions (Supplementary Tables 1 and 2). The root mean square deviation (RMSD) for the backbone α atoms when superposing **32**-wt to **32**-V30M was 0.21 Å, and the RMSD between **40**-wt and **40**-V30M was 0.25 Å. The superposition also indicated that the positions of the compounds in the T4-binding channels are completely identical with each other. Therefore, the V30M mutation does not affect the binding mode of the compounds in the T4-binding channels.

In all complexes, the electron densities of the compounds were clearly observed in the T4-binding channels (Fig. 2), as has been observed for typical stabilizers in previous studies.[3,4,9,10] The carboxyl

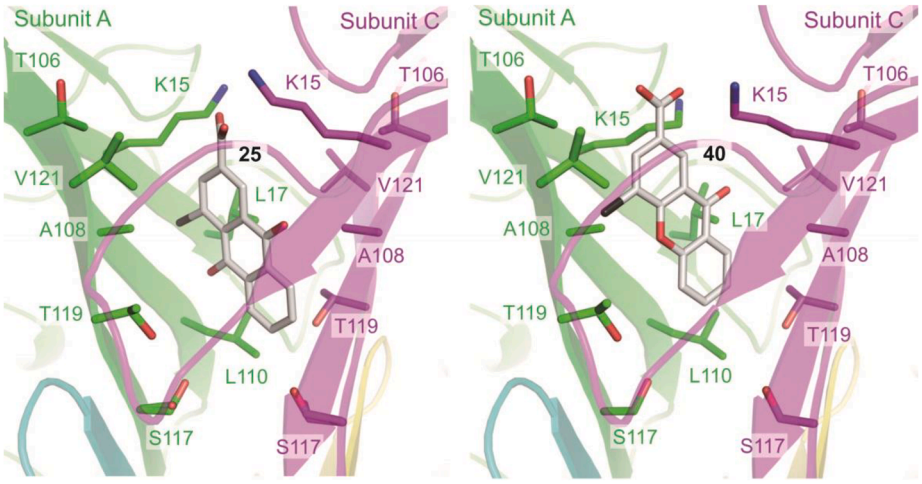

Fig. 3. Close-up view of the T4-binding channel of wild-type TTR in complex with **25** (left) and **40** (right). Oxygen, nitrogen, and chlorine atoms are colored red, blue and dark grey, respectively. The Leu17 side-chain in subunit C is omitted to show the compounds.

groups of **25**, **32** and **40** were close to Lys15 at the outer cavity, corroborating the importance of the electrostatic interaction with Lys15 (Figs. 2–4). This is consistent with the results of the amyloid inhibitory activity of **28** and **30**. Compound **30**, which has a carboxyl group at position 2, showed amyloid inhibitory activity, while compound **28**, in which the 2-COOH is replaced with a methyl group, showed no amyloid inhibitory activity (Fig. 1 and Table 1). A similar interaction has been observed in the crystal structures of TTR in complex with flufenamic acid, diflunisal, and tafamidis.[48–50] This favorable electrostatic interaction is important for the inhibition of the tetramer dissociation that is the rate-limiting step in the amyloid fibril formation of TTR.[50]

Compound **25** is an anthraquinone derivative, while **40** is a xanthone derivative, i.e., the only difference between **25** and **40** is located at position 10 (Fig. 1 and Table 1). However, the binding modes in the crystal structures of these two compounds are different (Fig. 3). Compound **25** in the **25**-TTR complex cannot adopt the binding mode observed in the **40**-TTR complex, probably due to the steric hindrance of the carbonyl oxygen at position 10 in the **25**-TTR complex. The ether oxygen at position 10 of **40** in the **40**-TTR complex is located near the T119 side chain (Fig. 3). The chlorine atom at position 4 of **40** is buried in a hydrophobic region formed by Leu17, Thr106, Ala108, Thr119, and Val121. There is no water molecule in the region around the chlorine atom and these side chains (Fig. 3). The interaction between 4-Cl of **40** and the surrounding hydrophobic region is important for the amyloid inhibitory activity: compound **40** with 4-Cl has stronger amyloid inhibitory activity than **30**, which has a hydrogen atom at position 4 (Fig. 1 and Table 1). The CLogP values of **30** and **40** are 2.85 and 3.60, respectively (Table 1). This indicates that the hydrophobically driven interaction between TTR and **40** mainly contributes to the strong inhibitory activity of **40**. Compounds **36**, **38**, and **39**, which are isomers of **40**, have similar amyloid inhibitory activity (Table 1). This indicates that a chlorine atom can be accommodated at positions 5, 7, and 8 (Figs. 1 and 3). On the other hand, the chlorine atom at position 4 in compound **25** interacts with a region formed by Lys15, Leu17, Ala108, Leu110 and T119 (Fig. 3). This interaction is important for the amyloid inhibitory activity of **25**. The amyloid inhibitory activity of **25** with 4-Cl is stronger than that of **18** without 4-Cl (Fig. 1 and Table 1). Compound **22**, in which 4-Cl is replaced with COOH, has no inhibitory activity, probably because the charged group cannot be accommodated in this hydrophobic space (Fig. 3). From the IC_{50} values of **18**, **22**, **23**, **25**, and **26**, the compounds with a methyl group (**23**) or chlorine (**25**) at position 4 have higher inhibitory activity than those with a hydrogen (**18**), carboxy group (**22**), or fluorine (**26**) at position 4 (Fig. 1 and Table 1). Comparing the CLogP values among **18**, **22**, **23**, **25**, and **26**, the compound with a relatively large CLogP value tends to have a strong inhibitory activity. This corroborates that the hydrophobic interaction at position 4 is important for the amyloid inhibitory activity. Comparing the IC_{50} values of **24** and **25**, compound **25**, which has one chlorine at

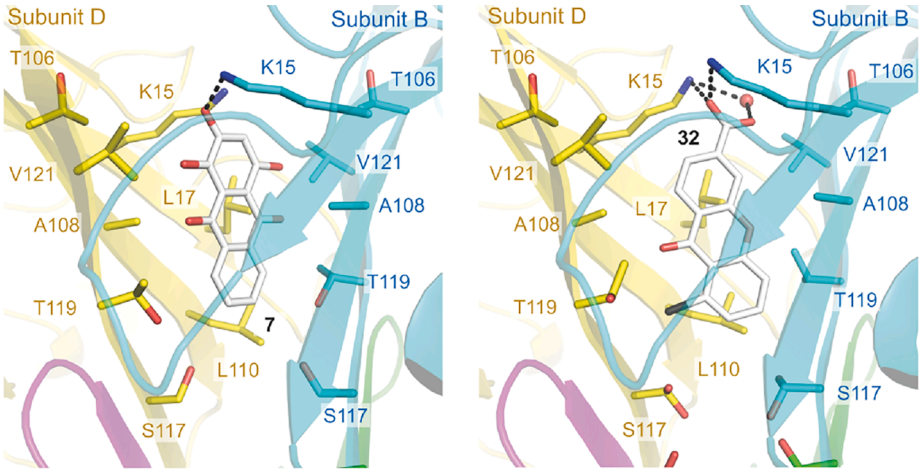

Fig. 4. Close-up view of the T4-binding channel of V30M-TTR in complex with **7** (left) and wild-type TTR in complex with **32** (right). Oxygen, nitrogen, and chlorine atoms are colored red, blue, and dark grey, respectively. The hydrogen-bond and salt-bridge are indicated by dashed lines. The red sphere is a water molecule.

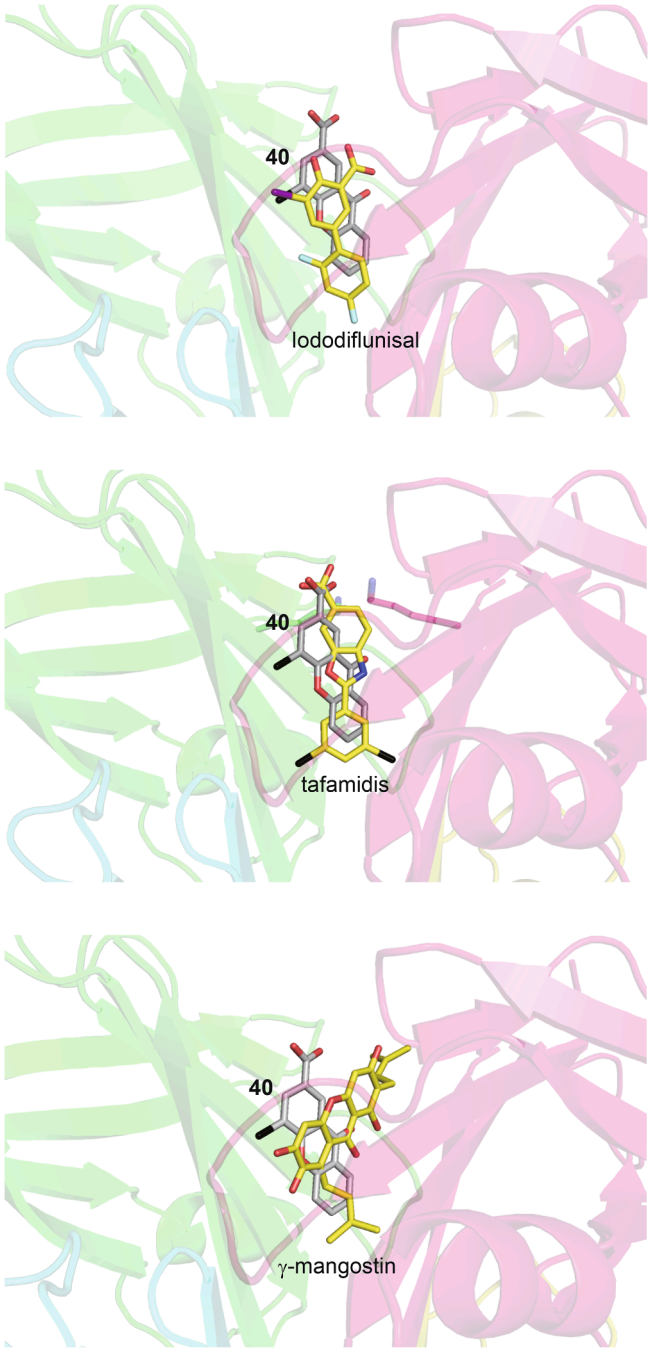

Fig. 5. A comparison of the binding direction of **40** with the known TTR stabilizers. The compound **40** is colored grey. Iododiflunisal (1Y1D), tafamidis (6E72), and γ-mangostin (4Y9E) are colored yellow. The chloride atoms are colored black. Oxygen, nitrogen, fluorine, and iodine are colored red, blue, light blue, and purple, respectively.

position 4, has higher inhibitory activity than **24**, which has multiple chlorines at positions 5, 6, 7, and 8 (Figs. 1 and 3 and Table 1).

We also determined the structures of TTR in complex with compounds **7** and **32**. In the **7**-TTR complex, the distance between the oxygen of the 2-OH of **7** and Lys15-N^{ζ} near the entrance of the T4-binding channel is 2.4 Å, suggesting the formation of a hydrogen bond. The importance of the 2-OH of **7** was also shown by the amyloid inhibitory activity of **7** and **13**. Compound **13**, which lacks the 2-OH of **7**, showed no amyloid inhibitory activity (Fig. 1 and Table 1). In the **32**-TTR complex, Lys15-N^{ζ} is close to the carboxyl group of **32**, which also suggests the formation of a salt bridge. One water molecule is trapped by the carboxyl group of **32** (Fig. 4). Moreover, 8-Cl of **32** is surrounded by the amino acid residues Leu110, Ser117, and Thr119, which are included in a region called halogen-binding pocket 3.[51] The 8-Cl of **32** contributes to the amyloid inhibitory activity, since the IC_{50} values of **31** and **32** are 19 μM and 10 μM, respectively (Fig. 1 and Table 1). On the other hand, compounds **32**, **33**, **34**, and **35** have similar levels of amyloid inhibitory activity (Table 1). This indicates that a chlorine atom can be accommodated at positions 5–8 in the ring without a carboxyl group (Figs. 1 and 4). Interestingly, the effect of the introduction of a chlorine atom at position 6 is different between **30** and **31**: compound **34** has amyloid inhibitory activity, while **37** has no inhibitory activity (Fig. 1 and Table 1). This indicates that the carboxyl group of **34** cannot be replaced from position 3 to position 2 (Figs. 1 and 4).

A previous study has revealed that iododiflunisal binds strongly to the T4-binding site of TTR and stabilizes the TTR tetramer better than diflunisal.[51] Previous crystallographic analysis has revealed that the iodine atom of iododiflunisal is located at the hydrophobic region, which is composed of Leu17, Thr106, Ala108, Thr119, and Val121.[51] The position of the chlorine atom in the complex of **40**-TTR was consistent with the position of the iodine atom in the complex of iododiflunisal and TTR (PDB code: 1Y1D): the distance between the iodine and chlorine atoms after alignment was only 0.4 Å (Fig. 5). These data suggest that the introduction of halogen substituents such as chlorine or iodine, which can be oriented to this hydrophobic space, significantly enhances the inhibitory activity of the stabilizers against amyloid aggregation.

Comparison of the binding mode between **40** and tafamidis revealed that the chlorine atom in **40** does not fit with those of tafamidis (Fig. 5). The chlorine of **40** is located near the entrance of the T4-binding channel. On the other hand, the two chlorine atoms of tafamidis are buried in the two symmetrical hydrophobic regions called halogen-binding pockets 3 and 3′, which are located in the inner channel.[50,51] The chlorine atom of **32** is also located in halogen-binding pocket 3 (Fig. 4). The removal of two chlorine atoms from tafamidis resulted in a substantial decrease of amyloid inhibitory activity.[50,52] Our results also indicated that the chlorine atom is important for the inhibitory activity of **32** (Fig. 1 and Table 1).

We have previously reported the X-ray crystal structure of TTR in complex with γ-mangostin, which is one of the xanthone derivatives.[37] The 2-dimethylallyl group of γ-mangostin is located near the entrance of the T4-binding channel (Fig. 1), and it interacts with the side chain of V121 via hydrophobic interaction.[37] The 8-dimethylallyl group is located in the channel, and it interacts with the side chains of A108, L110, S117 and T119. The 6-hydroxyl group undergoes water-mediated interaction with the side chains of Thr116 and Val121 (Fig. 1).[37] A chloride ion-mediated interaction takes place between the 7-hydroxyl group and the side chains of Ser117 and Thr119 in the structure of TTR in complex with γ-mangostin.[37] Because of the lack of these dimethylallyl and hydroxyl groups in **40**, the binding direction of **40** is quite different from that of γ-mangostin (Fig. 5).

2.4. *In vitro ADME assay and in vivo pharmacokinetic study*

An *in vitro* distribution, metabolism and elimination (ADME) assay is a standard method to evaluate the key physicochemical properties that are associated with the efficacy profile of a candidate compound. We performed a standard ADME assay of compounds **40** and **42**, which have the highest amyloid inhibitory activity among the xanthone derivatives (Table 2). The results were compared with those for tafamidis, which is the first approved drug for the treatment of familial amyloidotic polyneuropathy.[50]

The solubility was evaluated using Japanese Pharmacopoeia (JP) 1st test fluid and JP 2nd test fluid, and the results showed that the three compounds—**40**, **42** and tafamidis—were comparable. A parallel artificial membrane permeability assay (PAMPA) showed that **40** and **42** have good permeability properties. A PAMPA permeability assessment

has also been used to evaluate antipyrine and metoprolol, revealing that the two drugs have 100% and 95% gastrointestinal absorption in humans, respectively,[53] at values of 13 and 1.0 × 10^{-6} cm/*sec*. Since **40**, **42** and tafamidis are more permeable than antipyrine, it was inferred that all three agents were 100% absorbed in the gastrointestinal tract. In the metabolic stability test using rat liver microsomes, the residual rate after 30 min at 0.2 mg protein/mL was stable at around 88% for all three compounds, with and without the addition of NADPH, which is a coenzyme of CYP. The plasma protein-binding ratio of **40** is lower than that of tafamidis, while **42** showed a plasma protein-binding ratio similar to that of tafamidis. These results indicate that **40** and **42** have drug-like physicochemical properties that are similar to those of tafamidis (Table 2).

We also performed *in vivo* pharmacokinetics studies in rats using a liquid chromatography- tandem mass spectrometry (LC-MS/MS) method (Table 3). Compound solutions were injected intravenously (i.v.) or orally (p.o.) to male SD rats (n = 2). Blood samples were collected from the caudal vein at 5 (i.v.), 15, and 30 min and 1, 2, 4, and 8 h. The compound concentrations were determined by LC-MS/MS analysis of the supernatants of plasma samples. From the analysis of oral (p.o.) administration, the observed maximum peak plasma concentration was reached at approximately 2 h for **40**. On the other hand, compound **42** showed a maximum peak plasma concentration at approximately 0.25 h. The data of intravenous (i.v.) administration showed that the mean elimination half-lives were 1.7 h and 2.4 h for **40** and **42**, respectively, and both these half-lives were shorter than that of tafamidis (12 h). The estimated bioavailability (BA) of **40** was 69.8%, which is comparable with that of tafamidis. On the other hand, the BA of **42** is 34.9%, which is lower than that of **40** (Table 3). The main metabolic pathway of tafamidis is the formation of glucuronide conjugates for carboxyl groups (https://pfizerpro.jp/documents/if/vyn/vyn01if.pdf). Differences in metabolism other than CYP, such as differences in glucuronidation, may have contributed to the differences in the *in vivo* pharmacokinetic profiles of these three compounds.

After the final collection of the blood samples, the compound concentrations in the eyeball and the brain were determined by LC-MS/MS (Supplementary Table 3). Considering that the dose of tafamidis is one-tenth of those of **40** and **42**, the concentrations of **40** and **42** in the eyeball and brain were lower than those of tafamidis. We therefore concluded that it would be difficult to use **40** and **42** as therapeutics targeting TTR in the eye or brain. However, compounds **40** and **42** have drug-like properties similar to those of tafamidis (Tables 2 and 3), and thus they may have potential as therapeutic agents to stabilize TTR in the blood and thereby ameliorate TTR amyloidosis.

3. Conclusions

In this study, we investigated the amyloid inhibitory activities of anthraquinone and xanthone derivatives, and found that xanthone-2-carboxylic acid with a chlorine or methyl group at position 4 (**40** or **42**) has the highest amyloid inhibitory activity *in vitro*. X-ray crystallographic analysis of the **40**-TTR complex indicated the importance of the interaction of chlorine with the hydrophobic region formed by Leu17, Thr106, Ala108, Thr119, and Val121. An *in vitro* ADME assay and an *in vivo* pharmacokinetic analysis suggested that **40** and **42** have drug-like properties, although their elimination half-lives are shorter than that of tafamidis. Our results suggest that these compounds have potential as therapeutic agents to stabilize TTR in the blood.

4. Materials and methods

4.1. Chemistry

4.1.1. General

Chemicals were purchased from Sigma-Aldrich, Merck (Darmstadt, Germany), FUJIFILM Wako Chemicals (Osaka, JAPAN), Nacalai Tesque, Tokyo Chemical Industry (Tokyo), and Kanto Chemical (Tokyo) and used without further purification. Column chromatography was done on Cica silica gel 60 N (spherical, neutral; particle size, 63–210 nm; Kanto Chemical), while thin-layer chromatography was performed using Merck silica gel $60F_{254}$ plates. Melting points were taken on a Yanaco-micro melting point apparatus and are uncorrected. The nuclear magnetic resonance (NMR) spectra were acquired in the specified solvent by means of a JEOL JNM-A400 (400 and 100 MHz for ^{1}H and ^{13}C, respectively) or JEOL JNM-ECX500 (500 and 125 MHz for ^{1}H and ^{13}C, respectively). The chemical shifts (δ) are reported in ppm downfield from TMS, and coupling constants (*J*) are expressed in Hertz. IR spectra were measured with a JASCO FT/IR-460 Plus spectrophotometer (JASCO, Tokyo). The low-resolution mass spectra and high-resolution mass spectra were obtained with a Shimadzu GCMS-QP 500 (Shimadzu, Kyoto, Japan), JEOL D-200, or JEOL AX505 (JEOL, Tokyo) mass spectrometer in the electron impact mode at the ionization potential of 70 eV.

4.1.2. General procedure for construction of the anthraquinone skeleton

To a stirred solution of phthalic anhydride (290 mg, 1.96 mmol) in toluene (5 mL) was added anhydrous $AlCl_3$ (522 mg, 3.92 mmol) at 0 °C. The reaction mixture was stirred at 50 °C for 2 h. The reaction was quenched with water (5 mL), and the organic layer was separated. The aqueous layer was extracted with EtOAc (3 mL × 3). The organic layer and extracts were combined, dried over Na_2SO_4, and evaporated to give a white solid, which was used directly in the next step. The solution of the above solid in concentrated H_2SO_4 (2.0 mL) was heated to 100 °C for 1 h. After cooling, the reaction mixture was diluted with EtOAc (3 mL), and the organic layer was separated and washed with water (1 mL × 3). The organic layer was then dried over Na_2SO_4 and evaporated to give a pale yellow solid, which was recrystallized from EtOH to afford the corresponding anthraquinone **A1**–**A5** as a pale yellow solid.[42]

4.1.2.1. 2-Methylanthracene-9,10-dione (A1). Yield: 71%; ^{1}H NMR (400 MHz, $CDCl_3$) δ: 8.32–8.29 (2H, m), 8.21 (1H, d, *J* = 8.0 Hz), 8.11 (1H, s), 7.80–7.78 (2H, m), 7.60 (1H, dd, *J* = 8.0, 1.2 Hz), 2.54 (3H, s).[54]

4.1.2.2. 1,3-Dimethylanthracene-9,10-dione (A2). Yield: 76%; ^{1}H NMR (400 MHz, $CDCl_3$) δ: 8.26 (1H, dd, *J* = 7.2, 2.0 Hz), 8.26 (1H, dd, *J* = 7.2, 2.0 Hz), 8.05 (1H, s), 7.78 (1H, td, *J* = 7.2, 2.0 Hz), 7.74 (1H, td, *J* = 7.2, 2.0 Hz), 7.39 (1H, s), 2.83 (3H, s), 2.48 (3H, s).[55]

4.1.2.3. 1,2,3,4-Tetrachloro-6-methylanthracene-9,10-dione (A3). Yield: 15%; ^{1}H NMR (400 MHz, $CDCl_3$) δ: 8.06 (1H, d, *J* = 8.0 Hz), 7.95 (1H, s), 7.60 (1H, d, *J* = 8.0 Hz), 2.54 (3H, s).[56]

4.1.2.4. 1-Chloro-3-methylanthracene-9,10-dione (A4). Yield: 9%; ^{1}H NMR (400 MHz, $CDCl_3$) δ: 8.30 (1H, dd, *J* = 8.0, 1.6 Hz), 8.26 (1H, dd, *J* = 7.2, 2.0 Hz), 8.12 (1H, d, *J* = 1.2 Hz), 7.84–7.76 (2H, m), 7.63 (1H, s), 2.51 (3H, s); ^{13}C NMR (100 MHz, $CDCl_3$) δ: 182.41, 181.49, 145.13, 138.14, 135.61, 134.99, 134.44, 133.67, 132.34, 127.43, 127.34, 127.11, 126.69, 21.42; IR (KBr): 3952, 2363, 1676, 1591, 1306, 1275, 1246 cm^{-1}; mp: 196–197 °C; MS (EI) *m/z*: 256 (M^+); HRMS (EI) *m/z*: 256.0282 (M^+) [calcd for $C_{15}H_9ClO_2$: 256.0291].

4.1.2.5. 1-Fluoro-3-methylanthracene-9,10-dione (A5). Yield: 2%; ^{1}H NMR (400 MHz, $CDCl_3$) δ: 8.31–8.27 (2H, m), 7.98 (1H, s), 7.84–7.61 (2H, m), 7.30 (1H, d, *J* = 11.6 Hz), 2.54 (3H, s).[57]

4.1.3. General procedure for the synthesis of anthraquinone derivatives 18 and 21–26

4.1.3.1. Method A. To a stirred solution of the anthraquinone (**A1**–**A5**,

Table 2
Summary of *in vitro* ADME properties of **40** and **42**.

Compound	Aqueous Solubility (μM)		PAMPA Permeability ($\times 10^{-6}$ cm/s)	Hepatic Microsome Stability (mL/min/kg)	Plasma Protein Binding (% unbound)
	pH 1.2	pH 6.8			
40	2.9	>100	17	37.9	1.7
42	2.0	>100	18	35.7	0.73
tafamidis	0.088	>100	>50	38.7	0.51

0.14 mmol) in AcOH (1 mL) was added CrO_3 (104 mg, 1.04 mmol) at 0 °C, and the resulting mixture was refluxed for 18 h. After cooling, the reaction mixture was filtered through a pad of Celite and washed with EtOAc (1 mL × 3). The filtrate and washings were combined and evaporated to give a black solid, which was chromatographed on SiO_2 (5 g, CH_2Cl_2/MeOH = 50/1–5/1) to afford the corresponding anthraquinone derivatives as an orange solid.[43]

4.1.3.2. Method B. To a stirred solution of the anthraquinone (**A1**–**A5**, 0.52 mmol) in concentrated H_2SO_4 (3.0 mL) was added MnO_2 (272 mg, 3.12 mmol) at 0 °C, and the resulting mixture was heated at 60 °C for 20 h. After cooling, the reaction mixture was diluted with EtOAc (3 mL), and the organic layer was separated and washed with water (1 mL × 3). The organic layer was dried over Na_2SO_4 and evaporated to give a black solid, which was chromatographed on SiO_2 (5 g, CH_2Cl_2/MeOH = 50/1–5/1) to afford the corresponding anthraquinone derivatives as an orange solid.[44]

4.1.3.3. 9,10-Dioxo-9,10-dihydroanthracene-2-carboxylic acid (18). Yield: 41% (Method A); ^{1}H NMR (400 MHz, DMSO d_6) δ: 8.67 (1H, s), 8.40 (1H, dd, J = 8.0, 1.2 Hz), 8.31 (1H, d, J = 8.0 Hz), 8.26–8.22 (2H, m), 7.98–7.94 (2H, m).[58]

4.1.3.4. 3-Methyl-9,10-dioxo-9,10-dihydroanthracene-1-carboxylic acid (21). Yield: 54% (Method B); ^{1}H NMR (400 MHz, DMSO d_6) δ: 8.21–8.19 (1H, m), 8.16–8.14 (1H, m), 8.08 (1H, s), 7.93 (2H, m), 7.66 (1H, s), 2.52 (3H, s); ^{13}C NMR (100 MHz, DMSO d_6) δ: 182.15, 181.62, 170.19, 145.49, 136.28, 134.73, 134.56, 133.26, 133.05, 132.94, 132.66, 127.65, 127.09, 126.75, 21.14; IR (KBr): 3975, 2991, 2659, 2338, 1709, 1682, 1591, 1325, 1277, 1219 cm^{-1}; mp: 285–286 °C; MS (EI) *m/z*: 266 (M^+); HRMS (EI) *m/z*: 266.0585 (M^+) [Calcd for $C_{16}H_{10}O_4$: 266.0579].

4.1.3.5. 9,10-Dioxo-9,10-dihydroanthracene-1,3-dicarboxylic acid (22). Yield: 7% (Method B); ^{1}H NMR (400 MHz, $CDCl_3$) δ: 8.57 (1H, br), 8.21–8.19 (1H, m), 8.14–8.12 (1H, m), 8.02 (1H, br), 7.92–7.90 (2H, m).[59]

4.1.3.6. 4-Methyl-9,10-dioxo-9,10-dihydroanthracene-2-carboxylic acid (23). Yield: 19% (Method A); ^{1}H NMR (400 MHz, DMSO d_6) δ: 8.60 (1H, d, J = 1.6 Hz), 8.20–8.18 (3H, m), 7.96–7.89 (2H, m), 2.83 (3H, s); ^{13}C NMR (100 MHz, DMSO d_6) δ: 183.95, 182.14, 165.84, 141.80, 137.81, 134.72, 134.60, 134.35, 134.17, 134.13 133.19, 132.10, 126.88, 126.28, 125.85, 22.77; IR (KBr): 1701, 1676, 1593, 1269 cm^{-1}; mp: 272–273 °C; MS (EI) *m/z*: 266 (M^+); HRMS (EI) *m/z*: 266.0572 (M^+) [Calcd for $C_{16}H_{10}O_4$: 266.0579].

4.1.3.7. 5,6,7,8-Tetrachloro-9,10-dioxo-9,10-dihydroanthracene-2-carboxylic acid (24). Yield: 76% (Method A); ^{1}H NMR (400 MHz, DMSO d_6) δ: 8.51 (1H, d, J = 1.2 Hz), 8.36 (1H, dd, J = 8.0, 1.2 Hz), 8.18 (1H, d, J = 8.0 Hz).[56]

4.1.3.8. 4-Chloro-9,10-dioxo-9,10-dihydroanthracene-2-carboxylic acid (25). Yield: 61% (Method A); ^{1}H NMR (400 MHz, DMSO d_6) δ: 8.63 (1H, s), 8.28 (1H, d, J = 1.2 Hz), 8.19 (2H, m), 8.00–7.91 (2H, m); ^{13}C NMR (100 MHz, DMSO d_6) δ: 181.16, 180.94, 164.87, 136.92, 136.12, 135.67, 134.98, 134.39, 134.20, 133.83, 132.04, 131.75, 127.05, 126.48, 126.45; IR (KBr): 3086, 3072, 2982, 1701, 1680, 1589, 1302, 1261, 1178 cm^{-1}; mp: 249–250 °C; MS (EI) *m/z*: 286 (M^+); HRMS (EI) *m/z*: 286.0031 (M^+) [Calcd for $C_{15}H_7ClO_4$: 286.0033].

4.1.3.9. 4-Fluoro-9,10-dioxo-9,10-dihydroanthracene-2-carboxylic acid (26). Yield: 85% (Method A); ^{1}H NMR (400 MHz, DMSO d_6) δ: 8.50 (1H, s), 8.21–8.16 (2H, m), 8.05 (1H, d, J = 11.6 Hz), 7.96–7.90 (2H, m), 2.49 (3H, s); ^{13}C NMR (100 MHz, DMSO d_6) δ: 181.04, 180.15, 164.80, 161.97, 137.19, 137.11, 135.14, 134.90, 134.46, 133.64, 132.11, 126.67, 123.21, 122.87, 122.63; IR (KBr): 3971, 3751, 3636, 3094, 2361, 2328, 1678, 1612, 1591, 1570, 1470, 1423, 1223, 1165, 1047, 1022 cm^{-1}; mp: 224–225 °C; MS (EI) *m/z*: 270 (M^+); HRMS (EI) *m/z*: 270.0327 (M^+) [Calcd for $C_{15}H_7FO_4$: 270.0328].

4.1.3.10. 5-Acetyloxy-9,10-dioxo-9,10-dihydroanthracene-2-carboxylic acid (20). Anthraquinone **20** was prepared from 1-acetoxy-6-methylanthraquinone according to the literature.[45]

^{1}H NMR (400 MHz, DMSO d_6) δ: 8.63 (1H, d, J = 2.0 Hz), 8.38 (1H, dd, J = 8.0, 2.0 Hz), 8.22 (1H, d, J = 8.0 Hz), 8.21 (1H, dd, J = 8.0, 1.2 Hz), 7.98 (1H, t, J = 8.0 Hz), 7.66 (1H, dd, J = 8.0, 1.2 Hz), 2.42 (3H, s).

4.1.3.11. Synthesis of 5-Hydroxy-9,10-dioxo-9,10-dihydroanthracene-2-carboxylic acid (19). Anthraquinone **20** (20 mg, 0.06 mmol) was dissolved in 2.5% Na_2CO_3 aq. (1.0 mL). The resulting mixture was refluxed for 2 h. After cooling, the reaction mixture was acidified with 10% HCl aq. (2 mL). The aqueous mixture was extracted with CH_2Cl_2 (1 mL × 3). The organic extracts were combined, dried over Na_2SO_4, and evaporated to give a pale yellow solid, which was chromatographed on SiO_2 (5 g, CH_2Cl_2/MeOH = 50/1) to afford **19** (17 mg, 0.06 mmol, 98%) as a pale yellow solid.

^{1}H NMR (400 MHz, DMSO d_6) δ: 12.32 (1H, s), 8.64 (1H, d, J = 2.0 Hz), 8.41 (1H, d, J = 8.0 Hz), 8.34 (1H, d, J = 8.0 Hz), 7.85 (1H, dd, J = 8.4, 7.6 Hz), 7.77 (1H, dd, J = 7.6, 1.2 Hz), 7.43 (1H, dd, J = 8.4, 1.2 Hz).[60]

4.1.3.12. Synthesis of 5-Ethoxy-9,10-dioxo-9,10-dihydroanthracene-2-carboxylic acid (27). To a stirred solution of **20** (22 mg, 0.07 mmol) in EtOH (2.0 mL) was added concentrated H_2SO_4 (1 drop) at 0 °C, and the resulting mixture was refluxed for 18 h. After cooling, EtOH was evaporated and the residue was extracted with CH_2Cl_2 (1 mL × 3). The organic extracts were combined, dried over Na_2SO_4, and evaporated to give a pale yellow solid, which was used directly in the next step. To a stirred solution of the above ethyl ester in DMF (1 mL) were added Cs_2CO_3 (26 mg, 0.08 mmol) and EtI (0.01 mL, 0.10 mmol) at 0 °C, and the resulting mixture was heated at 60 °C for 20 h. After cooling, the reaction was quenched with water (3 mL), and then the aqueous mixture was extracted with Et_2O (1 mL × 3). The organic extracts were combined, dried over Na_2SO_4, and evaporated to give a yellow solid, which was used directly in the next step. To a stirred solution of the above ethyl ether in EtOH (1.5 mL) was added 10% NaOH aq. (1.5 mL) at room temperature, and the resulting mixture was refluxed for 22 h.

Table 3
Pharmacokinetic parameters of **40** and **42** from rat experiments.

Compound	Route	Dose (mg/kg)	C_0 or C_{max} (ng/mL)	T_{max} (h)	$t_{1/2}$ (h)	AUC_∞ (ng/mL·h)	CL_{tot} (mL/h/kg)	V_{dss} (mL/kg)	$AUC_{0\text{-}8h}$ (ng/mL·h)	BA (%)
40	i.v.	1	8650	–	1.7	13163	76	164		69.8
	p.o.	1	1124	2	5.0	9189	–	–		
42	i.v.	1	19229	–	2.4	7516	133	148		34.9
	p.o.	1	476	0.25	4.4	2625	–	–		
tafamidis	i.v.	0.1	537	–	12	4334	23	375	1714	55.8*
	p.o.	0.1	163	8	NC	NC	–	–	956	

NC: Not calculated.
BA: Bioavailability.
* The bioavailability of tafamidis was estimated from the value of AUC_{0-8h}.

After cooling, EtOH was evaporated and the residue was acidified with 10% HCl aq. (2 mL). The aqueous mixture was extracted with CH_2Cl_2 (1 mL × 3). The organic extracts were combined, dried over Na_2SO_4, and evaporated to give a pale yellow solid, which was chromatographed on SiO_2 (5 g, CH_2Cl_2/MeOH = 50/1) to afford **27** (12 mg, 0.04 mmol, 57% in 3 steps) as a yellow solid.

^{1}H NMR (500 MHz, $CDCl_3$) δ: 8.59 (1H, m), 8.35 (1H, dd, *J* = 8.0, 2.0 Hz), 8.20 (1H, d, *J* = 8.0 Hz), 7.85–7.82 (2H, m), 7.62–7.59 (1H, m), 4.26–4.22 (2H, m), 1.45–1.41 (3H, m); ^{13}C NMR (100 MHz, acetone d_6) δ: 182.47, 180.54, 165.54, 160.12, 137.85, 135.61, 135.43, 134.56, 132.69, 128.08, 127.54, 127.36, 124.28, 119.98, 119.19, 65.13, 14.23; IR (KBr): 3298.0, 3197.8, 3095.5, 2935.5, 1708.8, 1674.1, 1606.6, 1585.4, 1417.6, 1261.4, 1228.6, 1064.6 cm^{-1}; mp: 284–286 °C; MS (EI) *m/z*: 296 (M^+); HRMS (EI) *m/z*: 296.0695 (M^+) [calcd for $C_{14}H_9ClO_2$: 296.0685].

4.1.4. General procedure for construction of the xanthone skeleton

To a stirred solution of the corresponding *o*-nitrobenzaldehyde (1.32 mmol), PPh_3 (26 mg, 0.10 mmol), anhydrous $CuCl_2$ (9 mg, 0.07 mmol), and dried K_3PO_4 (618 mg, 2.91 mmol) in toluene (5 mL) were added to the corresponding phenol (1.72 mmol) at room temperature, and the resulting mixture was heated at 100 °C for 45 h under an air atmosphere. After cooling, the reaction was quenched with 10% NaOH aq. (5 mL) and the aqueous mixture was extracted with CH_2Cl_2 (5 mL × 3). The organic extracts were combined, dried over Na_2SO_4, and evaporated to give a black solid, which was chromatographed on SiO_2 (15 g, hexane/EtOAc = 50/1–5/1) to afford the corresponding xanthone as a pale yellow solid.[46]

4.1.4.1. 2-Methyl-9H-xanthen-9-one (28). Yield: 31%; ^{1}H NMR (400 MHz, $CDCl_3$) δ: 8.35 (1H, dd, *J* = 8.0, 2.0 Hz), 8.13 (1H, d, *J* = 2.0 Hz), 7.72 (1H, ddd, *J* = 8.4, 6.8, 2.0 Hz), 7.55 (1H, dd, *J* = 8.4, 2.0 Hz), 7.49 (1H, d, *J* = 8.4 Hz) , 7.41 (1H, d, *J* = 8.4 Hz), 7.38 (1H, ddd, *J* = 8.0, 6.8, 1.2 Hz), 2.48 (3H, s).[47]

4.1.4.2. 3-Methyl-9H-xanthen-9-one (29). Yield: 47%; ^{1}H NMR (400 MHz, $CDCl_3$) δ/ppm: 8.34 (1H, dd, *J* = 8.0, 1.2 Hz), 8.23 (1H, d, *J* = 8.0 Hz), 7.72 (1H, ddd, *J* = 8.0, 7.2, 1.2 Hz), 7.48 (1H, d, *J* = 8.0 Hz), 7.37 (1H, ddd, *J* = 8.0, 7.2, 1.2 Hz), 7.30 (1H, s), 7.20 (1H, d, *J* = 8.0 Hz).[47]

4.1.4.3. 1-Chloro-6-methyl-9H-xanthen-9-one (X1). Yield: 9%; ^{1}H NMR (400 MHz, $CDCl_3$) δ: 8.19 (1H, d, *J* = 8.0 Hz), 7.55 (1H, dd, *J* = 8.4, 8.0 Hz), 7.40 (1H, dd, *J* = 8.4, 1.2 Hz), 7.36 (1H, dd, *J* = 8.0, 1.2 Hz), 7.23 (1H, s), 7.19 (1H, dd, *J* = 8.0, 1.2 Hz), 2.50 (3H, s).[61]

4.1.4.4. 2-Chloro-6-methyl-9H-xanthen-9-one (X2). Yield: 11%; ^{1}H NMR (400 MHz, $CDCl_3$) δ: 8.29 (1H, d, *J* = 2.4 Hz), 8.21 (1H, d, *J* = 8.4 Hz), 7.65 (1H, dd, *J* = 9.2, 2.4 Hz), 7.45 (1H, d, *J* = 9.2 Hz), 7.30 (1H, s), 7.22 (1H, dd, *J* = 8.4, 1.2 Hz), 2.52 (3H, s).[62]

4.1.4.5. 3-Chloro-6-methyl-9H-xanthen-9-one (X3). Yield: 29%; ^{1}H NMR (400 MHz, $CDCl_3$) δ: 8.27 (1H, d, *J* = 8.8 Hz), 8.21 (1H, d, *J* = 8.4 Hz), 7.50 (1H, d, *J* = 2.0 Hz), 7.34 (1H, dd, *J* = 8.8, 2.0 Hz), 7.23 (1H, s), 7.22 (1H, dd, *J* = 8.4, 0.8 Hz), 2.52 (3H, s).[63]

4.1.4.6. 5-Chloro-3-methyl-9H-xanthen-9-one (X4). Yield: 33%; ^{1}H NMR (400 MHz, $CDCl_3$) δ: 8.25 (1H, dd, *J* = 8.0, 2.0 Hz), 8.21 (1H, d, *J* = 8.0 Hz), 7.78 (1H, dd, *J* = 8.0, 2.0 Hz), 7.43 (1H, s), 7.31 (1H, t, *J* = 8.0 Hz), 7.24 (1H, dd, *J* = 8.0, 1.2 Hz), 2.54 (3H, s); ^{13}C NMR (100 MHz, $CDCl_3$) δ: 176.13, 155.71, 151.55, 146.74, 134.58, 126.33, 125.91, 125.15, 123.58, 123.06, 122.61, 119.02, 117.85, 21.89; IR (KBr): 3836.2, 3745.5, 1670.2, 1627.8, 1600.8, 1467.7, 1438.8, 1313.4, 1238.2, 1180.4, 1151.4 cm^{-1}; mp: 164–165 °C; MS (EI) *m/z*: 244 (M^+); HRMS (EI) *m/z*: 244.0282 (M^+) [calcd for $C_{14}H_9ClO_2$: 244.0291].

4.1.4.7. 5-Chloro-2-methyl-9H-xanthen-9-one (X5). Yield: 21%; ^{1}H NMR (400 MHz, $CDCl_3$) δ: 8.26 (1H, d, *J* = 8.0 Hz), 8.12 (1H, s), 7.79 (1H, dd, *J* = 7.4, 1.6 Hz), 7.59 (1H, d, *J* = 8.8 Hz), 7.52 (1H, d, *J* = 8.8 Hz), 7.31 (1H, dd, *J* = 8.0, 7.4 Hz), 2.49 (3H, s).[64]

4.1.4.8. 6-Chloro-2-methyl-9H-xanthen-9-one (X6). Yield: 19%; ^{1}H NMR (400 MHz, $CDCl_3$) δ: 8.28 (1H, d, *J* = 8.4 Hz), 8.11 (1H, s), 7.56 (1H, dd, *J* = 8.8, 2.6 Hz), 7.51 (1H, d, *J* = 2.0 Hz), 7.40 (1H, d, *J* = 8.8 Hz), 7.34 (1H, dd, *J* = 8.4, 2.0 Hz), 2.48 (3H, s).[65]

4.1.4.9. 2-Chloro-7-methyl-9H-xanthen-9-one (X7). Yield: 23%; ^{1}H NMR (400 MHz, $CDCl_3$) δ/ppm: 8.30 (1H, d, *J* = 2.6 Hz), 8.11 (1H, s), 7.66 (1H, dd, *J* = 9.2, 2.6 Hz), 7.56 (1H, dd, *J* = 8.4, 2.6 Hz), 7.46 (1H, d, *J* = 9.2 Hz), 7.41 (1H, d, *J* = 8.4 Hz), 2.48 (3H, s).[66]

4.1.4.10. 1-Chloro-7-methyl-9H-xanthen-9-one (X8). Yield: 5%; ^{1}H NMR (400 MHz, $CDCl_3$) δ: 8.09 (1H, s), 7.56 (1H, dd, *J* = 8.4, 7.6 Hz), 7.52 (1H, dd, *J* = 8.8, 2.4 Hz), 7.41 (1H, dd, *J* = 8.4, 1.2 Hz), 7.37 (1H, d, *J* = 7.6 Hz), 7.34 (1H, d, *J* = 8.8 Hz), 2.47 (3H, s).[67]

4.1.4.11. 4-Chloro-2-methyl-9H-xanthen-9-one (X9). Yield: 18%; ^{1}H NMR (500 MHz, $CDCl_3$) δ: 8.33 (1H, dd, *J* = 8.0, 1.5 Hz), 8.05–8.04 (1H, m), 7.76 (1H, ddd, *J* = 8.0, 7.0, 1.5 Hz), 7.64 (1H, m), 7.61 (1H, d, *J* = 8.0 Hz), 7.41 (1H, ddd, *J* = 8.0, 7.0, 1.0 Hz), 2.46 (3H, s); ^{13}C NMR (100 MHz, $CDCl_3$) δ: 176.64, 155.80, 149.87, 135.96, 135.01, 134.01, 126.69, 124.84, 124.28, 122.64, 122.25, 121.35, 118.19, 20.68; IR (KBr): 3865, 1663, 1591, 1462, 1317, 1256, 1225, 1148, 1022 cm^{-1}; mp: 167–168 °C, MS (EI) *m/z*: 244 (M^+); HRMS (EI) *m/z*: 244.0292 (M^+) [calcd for $C_{14}H_9ClO_2$: 244.0291].

4.1.4.12. 4,5-Dichloro-2-methyl-9H-xanthen-9-one (X10). Yield: 18%; ^{1}H NMR (500 MHz, $CDCl_3$) δ: 8.24 (1H, dd, *J* = 8.0, 1.5 Hz), 8.03 (1H, m), 7.83 (1H, dd, *J* = 8.0, 1.5 Hz), 7.67 (1H, d, *J* = 2.5 Hz), 7.35 (1H, t, *J* = 8.0 Hz), 2.48 (3H, s); ^{13}C NMR (100 MHz, $CDCl_3$) δ: 176.07, 151.48, 149.63, 136.37, 135.19, 134.75, 125.24, 124.76, 124.23, 123.31, 122.81, 122.63, 122.20, 20.75; IR (KBr): 3894, 3751, 2328, 1665, 1564, 1437, 1377, 1308, 1186, 1126, 1067 cm^{-1}; mp: 254–255 °C; MS (EI) *m/z*: 278 (M^+); HRMS (EI) *m/z*: 277.9893 (M^+)

[calcd for $C_{14}H_8Cl_2O_2$: 277.9901].

4.1.4.13. 2,4-Dimethyl-9H-xanthen-9-one (X11). Yield: 26%; ^{1}H NMR (400 MHz, $CDCl_3$) δ: 8.34 (1H, dd, J = 8.0, 1.6 Hz), 7.98 (1H, s), 7.72 (1H, ddd, J = 8.4, 6.8, 1.6 Hz), 7.54 (1H, d, J = 8.4 Hz), 7.40 (1H, s), 7.37 (1H, ddd, J = 8.0, 6.8, 1.6 Hz), 2.54 (3H, s), 2.43 (3H, s).[68]

4.1.5. General procedure for the synthesis of xanthone derivatives 30–42

To a stirred solution of the xanthone (**28** or **29** or **X1**–**X11**, 0.11 mmol) in AcOH (1 mL)/Ac_2O (1 mL) was added CrO_3 (104 mg, 1.04 mmol) at 0 °C, and the resulting mixture was heated at 100 °C for 3 h. After cooling, the reaction mixture was filtered through a pad of Celite and washed with EtOAc (1 mL × 3). The filtrate and washings were combined and evaporated to give a black solid, which was chromatographed on SiO_2 (5 g, hexane/EtOAc = 5/1–1/1) to afford the corresponding xanthone derivatives as a white solid.

4.1.5.1. 9-Oxo-9H-xanthene-2-carboxylic acid (30). Yield: 79%; ^{1}H NMR (400 MHz, DMSO d_6) δ: 8.73 (1H, d, J = 2.0 Hz), 8.34 (1H, dd, J = 8.8, 2.0 Hz), 8.22 (1H, dd, J = 8.0, 2.0 Hz), 7.92 (1H, ddd, J = 8.4, 7.4, 2.0 Hz), 7.77 (1H, d, J = 8.8 Hz), 7.72 (1H, d, J = 8.4 Hz), 7.54 (1H, dd, J = 8.0, 7.4 Hz).[69]

4.1.5.2. 9-Oxo-9H-xanthene-3-carboxylic acid (31). Yield: 31%; ^{1}H NMR (400 MHz, DMSO d_6) δ: 8.29 (1H, d, J = 8.8 Hz), 8.21 (1H, dd, J = 8.0, 1.6 Hz), 8.10 (1H, s), 7.95 (1H, d, J = 8.8 Hz), 7.91 (1H, ddd, J = 8.8, 7.2, 1.6 Hz), 7.71 (1H, d, J = 8.8 Hz), 7.51 (1H, dd, J = 8.0, 7.2 Hz).[70]

4.1.5.3. 8-Chloro-9-oxo-9H-xanthene-3-carboxylic acid (32). Yield: 58%; ^{1}H NMR (400 MHz, DMSO d_6) δ: 8.23 (1H, d, J = 8.0 Hz), 8.04 (1H, s), 7.94 (1H, d, J = 8.0 Hz), 7.81 (1H, dd, J = 8.4, 8.0 Hz), 7.66 (1H, d, J = 8.4 Hz), 7.52 (1H, d, J = 8.0 Hz); ^{13}C NMR (100 MHz, DMSO d_6) δ: 174.62, 166.03, 157.51, 154.17, 137.28, 135.25, 132.70, 127.38, 126.81, 124.45, 124.31, 118.72, 118.20, 117.98; IR (KBr): 1699, 1668, 1597, 1495, 1456, 1425, 1323, 1292, 1167 cm^{-1}; mp: 281–282 °C; MS (EI) m/z: 274 (M^+); HRMS (EI) m/z: 274.0034 (M^+) [calcd for $C_{14}H_7ClO_4$: 274.0033].

4.1.5.4. 7-Chloro-9-oxo-9H-xanthene-3-carboxylic acid (33). Yield: 56%; ^{1}H NMR (400 MHz, DMSO d_6) δ: 8.29 (1H, d, J = 8.0 Hz), 8.13 (1H, d, J = 2.4 Hz), 8.10 (1H, d, J = 1.2 Hz), 7.97 (1H, dd, J = 8.0, 1.2 Hz), 7.95 (1H, dd, J = 9.2, 2.4 Hz), 7.78 (1H, d, J = 9.2 Hz).[70]

4.1.5.5. 6-Chloro-9-oxo-9H-xanthene-3-carboxylic acid (34). Yield: 71%; ^{1}H NMR (400 MHz, DMSO d_6) δ: 8.27 (1H, d, J = 7.6 Hz), 8.20 (1H, d, J = 8.4 Hz), 8.07 (1H, s), 7.97 (1H, d, J = 7.6 Hz), 7.91 (1H, s), 7.56 (1H, dd, J = 8.4, 2.4 Hz); ^{13}C NMR (100 MHz, $CDCl_3$) δ: 175.17, 165.92, 156.10, 155.22, 140.19, 137.12, 127.94, 126.70, 125.25, 124.60, 123.73, 120.15, 119.11, 118.25; IR (KBr): 2357, 1659, 1607, 1583, 1560, 1491, 1433, 1298, 1207, 1173, 1094, 1072 cm^{-1}; mp: >300 °C; MS (EI) m/z: 274 (M^+); HRMS (EI) m/z: 274.0031 (M^+) [calcd for $C_{14}H_7ClO_4$: 274.0033].

4.1.5.6. 5-Chloro-9-oxo-9H-xanthene-3-carboxylic acid (35). Yield: 83%; ^{1}H NMR (400 MHz, DMSO d_6) δ: 8.29 (1H, d, J = 8.4 Hz), 8.16 (1H, dd, J = 7.6, 1.6 Hz), 8.12 (1H, s), 8.08 (1H, dd, J = 8.0, 1.6 Hz), 7.99 (1H, dd, J = 8.4, 1.2 Hz), 7.50 (1H, dd, J = 8.0, 7.6 Hz); ^{13}C NMR (100 MHz, DMSO d_6) δ: 175.26, 165.82, 154.82, 151.26, 137.17, 135.68, 126.74, 125.04, 124.90, 124.76, 123.38, 122.74, 121.79, 119.10; IR (KBr): 3065, 1703, 1674, 1603, 1495, 1474, 1429, 1304, 1209, 1177 cm^{-1}; mp: >300 °C; MS (EI) m/z: 274 (M^+), HRMS (EI) m/z: 274.0034 (M^+) [calcd for $C_{14}H_7ClO_4$: 274.0033].

4.1.5.7. 5-Chloro-9-oxo-9H-xanthene-2-carboxylic acid (36). Yield: 68%; ^{1}H NMR (400 MHz, DMSO d_6) δ: 8.71 (1H, d, J = 2.4 Hz), 8.36 (1H, dd, J = 8.8, 2.4 Hz), 8.17 (1H, dd, J = 8.0, 2.0 Hz), 8.09 (1H, dd, J = 8.0, 2.0 Hz), 7.83 (1H, d, J = 8.8 Hz), 7.51 (1H, t, J = 8.0 Hz); ^{13}C NMR (100 MHz, DMSO d_6) δ: 175.32, 166.00, 157.63, 151.04, 135.82, 135.74, 127.83, 127.24, 125.13, 125.10, 122.69, 121.81, 120.66, 119.02; IR (KBr): 3155, 3038, 1730, 1645, 1616, 1603, 1489, 1470, 1435, 1312 cm^{-1}; mp: >300 °C; MS (EI) m/z: 274 (M^+); HRMS (EI) m/z: 274.0026 (M^+) [calcd for $C_{14}H_7ClO_4$: 274.0033].

4.1.5.8. 6-Chloro-9-oxo-9H-xanthene-2-carboxylic acid (37). Yield: 53%; ^{1}H NMR (400 MHz, DMSO d_6) δ: 8.71 (1H, d, J = 2.4 Hz), 8.35 (1H, dd, J = 8.8, 2.4 Hz), 8.20 (1H, d, J = 8.8 Hz), 7.93 (1H, d, J = 1.6 Hz), 7.76 (1H, d, J = 8.8 Hz), 7.57 (1H, dd, J = 8.8, 1.6 Hz); ^{13}C NMR (100 MHz, DMSO d_6) δ: 175.43, 166.56, 157.56, 157.46, 155.97, 140.13, 136.09, 128.04, 127.51, 125.37, 120.76, 120.15, 118.46, 118.33; IR (KBr): 3414, 2922, 1676, 1605, 1445, 1425, 1261 cm^{-1}; mp: >300 °C; MS (EI) m/z: 274 (M^+); HRMS (EI) m/z: 274.0034 (M^+) [calcd for $C_{14}H_7ClO_4$: 274.0033].

4.1.5.9. 7-Chloro-9-oxo-9H-xanthene-2-carboxylic acid (38). Yield: 26%; ^{1}H NMR (400 MHz, DMSO d_6) δ: 8.69 (1H, d, J = 2.4 Hz), 8.34 (1H, dd, J = 8.8, 2.4 Hz), 8.11 (1H, d, J = 2.8 Hz), 7.94 (1H, dd, J = 8.4, 2.8 Hz), 7.76 (1H, d, J = 8.4 Hz), 7.76 (1H, d, J = 8.8 Hz).[61]

4.1.5.10. 8-Chloro-9-oxo-9H-xanthene-2-carboxylic acid (39). Yield: 42%; ^{1}H NMR (400 MHz, DMSO d_6) δ: 8.67 (1H, d, J = 2.4 Hz), 8.31 (1H, dd, J = 8.8, 2.4 Hz), 7.82 (1H, dd, J = 8.4, 8.0 Hz), 7.71 (1H, d, J = 8.8 Hz), 7.67 (1H, d, J = 8.4 Hz), 7.54 (1H, dd, J = 8.0, 1.2 Hz); ^{13}C NMR (100 MHz, DMSO d_6) δ: 174.43, 166.09, 157.17, 156.92, 135.46, 135.24, 132.73, 128.04, 127.60, 126.90, 121.48, 118.41, 118.07, 117.93; IR (KBr): 3555, 3483, 3414, 3364, 2332, 1674, 1601, 1493, 1429, 1279, 1173, 1128 cm^{-1}; mp: >300 °C; MS (EI) m/z: 274 (M^+); HRMS (EI) m/z: 274.0034 (M^+) [calcd for $C_{14}H_7ClO_4$: 274.0033].

4.1.5.11. 4-Chloro-9-oxo-9H-xanthene-2-carboxylic acid (40). Yield: 54%; ^{1}H NMR (400 MHz, DMSO d_6) δ: 8.58 (1H, d, J = 1.6 Hz), 8.34 (1H, s), 8.17 (1H, d, J = 6.8 Hz), 7.92 (1H, br), 7.73 (1H, d, J = 7.6 Hz), 7.54 (1H, br); ^{13}C NMR (100 MHz, DMSO d_6) δ: 175.24, 165.23, 155.14, 153.58, 136.32, 134.75, 126.97, 126.34, 126.14, 125.52, 122.32, 122.26, 120.78, 118.41; IR (KBr): 3566, 3192, 3045, 2448, 2357, 2332, 1674, 1599, 1560, 1489, 1464, 1250, 1211, 1180, 1153, 1113, 1088 cm^{-1}; mp: >300 °C; MS (EI) m/z: 274 (M^+); HRMS (EI) m/z: 274.0034 (M^+) [calcd for $C_{14}H_7ClO_4$: 274.0033].

4.1.5.12. 4,5-Dichloro-9-oxo-9H-xanthene-2-carboxylic acid (41). Yield: 61%; ^{1}H NMR (400 MHz, DMSO d_6) δ: 8.58 (1H, d, J = 2.0 Hz), 8.40 (1H, d, J = 2.0 Hz), 8.14 (1H, dd, J = 8.0, 2.0 Hz), 8.10 (1H, dd, J = 8.0, 2.0 Hz), 7.53 (1H, td, J = 8.0, 2.0 Hz); ^{13}C NMR (100 MHz, DMSO d_6) δ: 174.98, 165.18, 153.36, 150.78, 136.05, 135.04, 127.42, 126.29, 125.74, 125.15, 122.66, 122.47, 122.18, 122.10; IR (KBr): 3906, 3751, 3076, 2357, 2343, 2330, 1682, 1601, 1582, 1468, 1410, 1279, 1225, 1190, 1146 cm^{-1}; mp: >300 °C; MS (EI) m/z: 308 (M^+); HRMS (EI) m/z: 307.9644 (M^+) [calcd for $C_{14}H_6Cl_2O_4$: 307.9643].

4.1.5.13. 4-Methyl-9-oxo-9H-xanthene-2-carboxylic acid (42). Yield: 99%; ^{1}H NMR (400 MHz, DMSO d_6) δ: 13.24 (1H, br), 8.58 (1H, s), 8.24 (1H, s), 8.20 (1H, d, J = 7.6 Hz), 7.92 (1H, dd, J = 8.4, 8.0 Hz), 7.75 (1H, d, J = 8.4 Hz), 7.52 (1H, dd, J = 8.0, 7.6 Hz), 2.58 (3H, s); ^{13}C NMR (100 MHz, DMSO d_6) δ: 176.03, 166.32, 156.49, 155.40, 135.90, 135.81, 128.06, 126.00, 125.98, 125.50, 124.93, 120.84, 120.64, 118.50, 15.32; IR (KBr): 2370, 2353, 2324, 1697, 1663, 1606, 1597, 1470, 1431, 1406, 1321, 1292, 1225 cm^{-1}; mp: >300 °C; MS (EI) m/z: 254 (M^+); HRMS (EI) m/z: 254.0588 (M^+) [calcd for $C_{15}H_{10}O_4$:

254.0579].

4.2. Materials

Wild-type TTR and V30M were expressed in *Escherichia coli* as described previously.[71] Chrysazin (**1**), Emodin (**3**), Aloe Emodin (**5**), Alizarin Safirol SE (**11**), Nuclear Fast Red (**12**), Leucoquinizarin (**14**), Anthrarufin (**15**), Diacerein (**16**) and Daunorubicin Hydrochloride (**17**) were purchased from Tokyo Chemical Industry Co. Chrysophanol (**2**), Physcion (**4**) and Purpurin (**7**) were purchased from LKT Laboratories. Isopurpurin (**9**) and Quinizarin (**13**) were purchased from Sigma-Aldrich Japan. Rhein (**6**), Alizarin (**8**) and Quinalizarin (**10**) were purchased from AdooQ-BioScience, FUJIFILM Wako Pure Chemical, and Vitas-M Laboratory, respectively.

4.3. Protein crystallography

For the preparation of TTR and inhibitor complexes, 30 mg/mL WT-TTR or V30M-TTR and 10 mM of compound **7**, **25**, **32** or **40** (in DMSO) were mixed in a 9:1 ratio, and the protein samples were incubated for 60 min at room temperature. Single crystals suitable for a diffraction experiment were successfully obtained by the sitting-drop vapor-diffusion method under the condition [15–26% polyethylene glycol 400, 0.4 M $CaCl_2$, 0.1 M sodium acetate pH 4.9]. Crystals were cryo-protected by the buffer [32% polyethylene glycol 400, 0.4 M $CaCl_2$, 0.1 M sodium acetate pH 5.0] and flash-frozen using liquid nitrogen. X-ray diffraction data were collected using beamlines 5A and 17A at the Photon Factory (Tsukuba, Japan). The diffraction data sets were processed with XDS.[72] All crystals were isomorphous with typical TTR crystal structures with space group $P2_12_12$. Therefore, structure refinements were directly performed without molecular replacement phasing using the apo V30M-TTR (PDB ID: 4PWE) or apo WT-TTR (PDB ID: 4 N85) structures as initial models.[39,40] The structures were refined using PHENIX.REFINE with manual model building using COOT.[73,74] The 3D structures and library data of the inhibitors were created using PRODRG {Schuttelkopf, 2004 #1122}. Because the inhibitor-binding sites were located on the crystallographic symmetry axis, the inhibitors were refined at 50% occupancy (Fig. 2). The coordinates and structure factors have been deposited in the Protein Data Bank (Supplementary Tables 1 and 2).

4.4. Acid-Mediated aggregation experiments

V30M-TTR was incubated at pH 7.0 in the presence of the compounds for 30 min at room temperature prior to protein aggregation. Acid-mediated protein aggregation was initiated by diluting the protein solution with 100 mM acetate buffer at pH 4.6. The protein concentration was set to 10 μM and the compound concentration was set to 0–100 μM. After incubation for 96 h at pH 4.6 and 37 °C, the solution was 6-fold diluted with 200 mM Tris-HCl at pH 8.0 containing 20 μM thioflavin T. The fluorescence measurement was performed as described previously.[39] The IC_{50} values were obtained by fitting the data with the 4-parameter logistic model.[75] At least two technical replicates were performed.

4.5. Animals

Male Sprague Dawley rats (7-week-old) were purchased from SLC Inc. (Hamamatsu, Japan). All animals were maintained in air-conditioned quarters with a room temperature of 20 ± 2 °C, relative humidity of 50 ± 10%, and an alternating 12 h light:dark cycle. The rats were fed a certified diet (MF; Oriental Yeast Co.) and water ad libitum. The studies were conducted in accordance with the guidelines provided by the Animal Care and Use Committee of Osaka University.

4.6. ADME assay

Solubility assay: The Japanese Pharmacopeia (JP) 1st fluid (pH 1.2) or JP 2nd fluid (pH 6.8) for dissolution testing was used for solubility measurements. A test solution of the test compound was prepared by diluting 10 mM DMSO stock solution 2 μL:165 μL in JP 1st or 2nd fluid and mixed at 37 °C for 4 h by rotation at 1000 rpm. After loading the mixed solution into 96-well MultiScreen Filter Plates (product number MSHVN4510, 0.45 μm hydrophilic PVDF membrane; Millipore, Bedford, MA), filtration was performed by centrifugation. The filtrates were mixed with acetonitrile and analyzed by HPLC-UV (254 nm). Solubility was calculated by comparing the peak area of the filtrate mixture with that of a 100 μM standard solution. When the peak area of the filtrate mixture was larger than the peak area of the standard solution, it was described as >100 μM. At least two technical replicates were performed.

A PAMPA assay was performed to determine the passive membrane diffusion rates: A Corning Gentest Pre-coated PAMPA Plate System was used in the PAMPA permeability test. The acceptor plate was prepared by adding 200 μL of 5% DMSO/0.1 M phosphate buffer (pH7.4) to each well, and then 300 μL of 10 μM test compounds in 5% DMSO/0.1 M phosphate buffer (pH 6.4) was added to the donor wells. The acceptor plate was then placed on top of the donor plate and incubated at 37 °C without agitation for 4 h. At the end of the incubation, the plates were separated and the solutions from each well of both the acceptor plate and the donor plate were transferred to 96-well plates and mixed with acetonitrile. The final concentrations of compounds in both the donor wells and acceptor wells, as well as the concentrations of the initial donor solutions, were analyzed by liquid chromatography tandem mass spectrometry (LC-MS/MS). The permeability of the compounds was calculated according to a previous report.[53] The recovery of tested compounds was more than 90%. The permeabilities of antipyrine (100 μM), metoprolol (500 μM) and sulfasalazine (500 μM) as reference compounds were 13, 1.0 and 0.044 × 10^{-6} cm/s, respectively. At least two technical replicates were performed.

Hepatic microsomal stability assay: Disappearance of the parent compound over time was measured by using the amount of drug at time zero as a reference. After 5 min of preincubation, 1 mM NADPH (final concentration; the same applies to the following) was added to a mixture containing 1 μM of the test compound, 0.2 mg/mL of rat liver microsomes (Sekisui XenoTech LLC, Kansas City, KS), 1 mM EDTA and 0.1 M phosphate buffer (pH 7.4) and incubated at 37 °C for 30 min with rotation at 60 rpm. An aliquot of 50 μL of the incubation mixture was sampled and added to 250 μL of chilled acetonitrile/internal standard (IS). After centrifuging for 15 min at 3150*g* (4 °C), the supernatants were analyzed by LC-MS/MS. Hepatic microsomal stability (mL/min/kg, CLint) was calculated according to a previous report,[76] using 44.8 mg MS protein/g liver and 40.0 g liver/kg body weight as scaling factors. At least two technical replicates were performed.

Determination of the unbound fraction in rat plasma: An equilibrium dialysis apparatus was used to determine the unbound fraction for each compound in rat plasma. A Rapid Equilibrium Dialysis (RED) Device Single-Use Plate with Inserts, 8 K MWCO (ThermoFisher Scientific, Waltham, MA) was used. Plasma was spiked with the test compound (1 μM), and 200 μL aliquots were loaded into the apparatus and dialyzed versus 350 μL of 0.1 M phosphate buffer (pH 7.4) at 37 °C for 4 h by rotation at 1000 rpm. The unbound fraction was calculated as the ratio of receiver side (buffer) to donor side (plasma) concentrations. At least two technical replicates were performed.

4.7. In vivo pharmacokinetics assay

A test compound solution in 10% DMSO/0.1 M phosphate buffer (pH 8.5) was injected intravenously (i.v.) or orally (p.o.) to male SD rats. The dosage of the test compounds was 0.1 (tafamidis) or 1 (**40** and **42**) mg/5 mL/kg. Blood samples were collected from the caudal vein at 5 (i.

v.), 15, and 30 min and 1, 2, 4, and 8 h. Plasma was prepared by centrifugation of the blood samples at −80 °C. Plasma samples were precipitated with 4 volumes of acetonitrile/IS and centrifuged at 15,000*g* at 4 °C for 10 min. The supernatants were analyzed by LC-MS/MS. Standard non-compartmental analysis was performed to determine the pharmacokinetic parameters: the estimated initial concentration (C_0), maximum plasma concentration (C_{max}), time to maximum plasma concentration (T_{max}), elimination half-life ($t_{1/2}$), area under the concentration time curve from time zero to infinity (AUC_∞), AUC from time zero to 8 h ($AUC_{0\text{-}8h}$), total clearance (CL_{tot}), and volume of distribution at steady-state (V_{dss}). The absolute bioavailability (BA) of the oral dose was calculated as AUC_∞(p.o.)/AUC_∞(i.v.). At least two biological replicates were generated for each sample.

4.8. LC-MS/MS quantification Method

An LC-MS8060 instrument equipped with a Shimadzu Nexera series LC system (Shimadzu, Kyoto, Japan) was used. All compounds were analyzed in multi-reaction monitoring mode under electron spray ionization conditions. The analytical column used was a CAPCELLPAK C18 MGIII (3 μm × 2.0 mm ID × 35 mm; OSAKA SODA, Osaka, Japan) at 50 °C. The gradient mobile phase consisted of 0.1% formic acid in water (mobile phase A) and 0.1% formic acid in acetonitrile (mobile phase B) at a total flow rate of 1 mL/min. The initial mobile phase composition was 10% B, which was held constant for 0.5 min, increased in a linear fashion to 90% B over 1 min, then held constant for 0.8 min, and finally brought back to the initial condition of 10% B over 0.01 min and re-equilibrated for 1 min. The transitions (precursor ion > product ion) of tafamidis, **40**, **42**, and IS (methyl testosterone) are 306.0 > 262.1, 273.0 > 229.1 (negative), 255.1 > 211.2, and 303.1 > 109.1 (positive), respectively.

Declaration of Competing Interest

The authors declare that they have no known competing financial interests or personal relationships that could have appeared to influence the work reported in this paper.

Acknowledgments

This research was supported by AMED under grant number JP20lm0203011. This research was partially supported by the Platform Project for Supporting Drug Discovery and Life Science Research (Basis for Supporting Innovative Drug Discovery and Life Science Research (BINDS)) from AMED under grant numbers JP20am0101087 and JP20am0101123 (support number 2110).

Author contributions

T.Y., N.T. and M.M. designed the project. T.Y. and R.K. performed the X-ray crystallography. R.K. analyzed the inhibitory activity of the compounds. K.I., Y.N., Y.S. and T.O. synthesized the compounds. W.K. performed the ITC measurements. K.K. and S.N. performed *in vitro* ADME and *in vivo* pharmacokinetic study. T.Y., K.K., N.T. and M.M. prepared the manuscript based on discussions among all the authors.

Appendix A. Supplementary data

Supplementary data to this article can be found online at https://doi.org/10.1016/j.bmc.2021.116292.

References

1 Benson MD, Buxbaum JN, Eisenberg DS, et al. Amyloid nomenclature 2018: recommendations by the International Society of Amyloidosis (ISA) nomenclature committee. *Amyloid.* 2018;25:215–219.
2 Vatassery GT, Quach HT, Smith WE, Benson BA, Eckfeldt JH. A sensitive assay of transthyretin (prealbumin) in human cerebrospinal fluid in nanogram amounts by ELISA. *Clin Chim Acta.* 1991;197:19–25.
3 Johnson SM, Wiseman RL, Sekijima Y, Green NS, Adamski-Werner SL, Kelly JW. Native state kinetic stabilization as a strategy to ameliorate protein misfolding diseases: a focus on the transthyretin amyloidoses. *Acc Chem Res.* 2005;38:911–921.
4 Johnson SM, Connelly S, Fearns C, Powers ET, Kelly JW. The transthyretin amyloidoses: from delineating the molecular mechanism of aggregation linked to pathology to a regulatory-agency-approved drug. *J Mol Biol.* 2012;421:185–203.
5 Vieira M, Saraiva MJ. Transthyretin: a multifaceted protein. *Biomol Concepts.* 2014;5:45–54.
6 Galant NJ, Westermark P, Higaki JN, Chakrabartty A. Transthyretin amyloidosis: an under-recognized neuropathy and cardiomyopathy. *Clin Sci (Lond).* 2017;131:395–409.
7 Ando Y, Coelho T, Berk JL, et al. Guideline of transthyretin-related hereditary amyloidosis for clinicians. *Orphanet J Rare Dis.* 2013;8:31.
8 Ueda M, Ando Y. Recent advances in transthyretin amyloidosis therapy. *Transl Neurodegener.* 2014;3:19.
9 Yokoyama T, Mizuguchi M. Inhibition of the amyloidogenesis of transthyretin by natural products and synthetic compounds. *Biol Pharm Bull.* 2018;41:979–984.
10 Yokoyama T, Mizuguchi M. Transthyretin amyloidogenesis inhibitors: from discovery to current developments. *J Med Chem.* 2020;63:14228–14242.
11 Coelho T, Maia LF, Martins da Silva A, et al. Tafamidis for transthyretin familial amyloid polyneuropathy: a randomized, controlled trial. *Neurology.* 2012;79:785–792.
12 Coelho T, Maia LF, da Silva AM, et al. Long-term effects of tafamidis for the treatment of transthyretin familial amyloid polyneuropathy. *J Neurol.* 2013;260:2802–2814.
13 Berk JL, Suhr OB, Obici L, et al. Diflunisal Trial Consortium. Repurposing diflunisal for familial amyloid polyneuropathy: a randomized clinical trial. *JAMA.* 2013;310:2658–2667.
14 Gamez J, Salvadó M, Reig N, et al. Transthyretin stabilization activity of the catechol-O-methyltransferase inhibitor tolcapone (SOM0226) in hereditary ATTR amyloidosis patients and asymptomatic carriers: proof-of-concept study. *Amyloid.* 2019;26:74–84.
15 Pinheiro F, Varejão N, Esperante S, et al. Tolcapone, a potent aggregation inhibitor for the treatment of familial leptomeningeal amyloidosis. *FEBS J.* 2021;288:310–324.
16 Fox JC, Hellawell JL, Rao S, et al. First-in-human study of AG10, a novel, oral, specific, selective, and potent transthyretin stabilizer for the treatment of transthyretin amyloidosis: a phase 1 safety, tolerability, pharmacokinetic, and pharmacodynamic study in healthy adult volunteers. *Clin Pharmacol Drug Dev.* 2020;9:115–129.
17 Vidal R, Garzuly F, Budka H, et al. Meningocerebrovascular amyloidosis associated with a novel transthyretin mis-sense mutation at codon 18 (TTRD 18G). *Am J Pathol.* 1996;148:361–366.
18 Benson MD. Leptomeningeal amyloid and variant transthyretins. *Am J Pathol.* 1996;148:351–354.
19 Brett M, Persey MR, Reilly MM, et al. Transthyretin Leu12Pro is associated with systemic, neuropathic and leptomeningeal amyloidosis. *Brain.* 1999;122:183–190.
20 Nakagawa K, Sheikh SI, Snuderl M, Frosch MP, Greenberg SM. A new Thr49Pro transthyretin gene mutation associated with leptomeningeal amyloidosis. *J Neurol Sci.* 2008;272:186–190.
21 Llull L, Berenguer J, Yagüe J, Graus F. Leptomeningeal amyloidosis due to A25T TTR mutation: a case report. *Neurologia.* 2014;29:382–384.
22 Sekijima Y. Transthyretin-type cerebral amyloid angiopathy: a serious complication in post-transplant patients with familial amyloid polyneuropathy. *J Neurol Neurosurg Psychiatry.* 2015;86:124.
23 Beirão JM, Malheiro J, Lemos C, Beirão I, Costa P, Torres P. Ophthalmological manifestations in hereditary transthyretin (ATTR V30M) carriers: a review of 513 cases. *Amyloid.* 2015;22:117–122.
24 Maia LF, Magalhães R, Freitas J, et al. CNS involvement in V30M transthyretin amyloidosis: clinical, neuropathological and biochemical findings. *J Neurol Neurosurg Psychiatry.* 2015;86:159–167.
25 Lozeron P, Théaudin M, Mincheva Z, Ducot B, Lacroix C, Adams D. French Network for FAP (CORNAMYL). Effect on disability and safety of Tafamidis in late onset of Met30 transthyretin familial amyloid polyneuropathy. *Eur J Neurol.* 2013;20:1539–1545.
26 Loconte V, Menozzi I, Ferrari A, et al. Structure-activity relationships of flurbiprofen analogues as stabilizers of the amyloidogenic protein transthyretin. *J Struct Biol.* 2019;208:165–173.
27 Yokoyama T, Mizuguchi M. Crown ethers as transthyretin amyloidogenesis inhibitors. *J Med Chem.* 2019;62:2076–2082.
28 Cotrina EY, Oliveira Â, Leite JP, et al. Repurposing benzbromarone for familial amyloid polyneuropathy: a new transthyretin tetramer stabilizer. *Int J Mol Sci.* 2020;21:7166.
29 Ciccone L, Nencetti S, Tonali N, et al. Monoaryl derivatives as transthyretin fibril formation inhibitors: design, synthesis, biological evaluation and structural analysis. *Bioorg Med Chem.* 2020;28, 115673.
30 Kim B, Ko YH, Runfola M, et al. Diphenyl-methane based thyromimetic inhibitors for transthyretin amyloidosis. *Int J Mol Sci.* 2021;22:3488.
31 Gong H, He Z, Peng A, et al. Effects of several quinones on insulin aggregation. *Sci Rep.* 2014;4:5648.
32 Malik EM, Müller CE. Anthraquinones As pharmacological tools and drugs. *Med Res Rev.* 2016;36:705–748.
33 Baures PW, Peterson SA, Kelly JW. Discovering transthyretin amyloid fibril inhibitors by limited screening. *Bioorg Med Chem.* 1998;6:1389–1401.

34 Pickhardt M, Gazova Z, von Bergen M, et al. Anthraquinones inhibit tau aggregation and dissolve Alzheimer's paired helical filaments in vitro and in cells. *J Biol Chem.* 2005;280:3628–3635.
35 Maia F, Almeida Mdo R, Gales L, et al. The binding of xanthone derivatives to transthyretin. *Biochem Pharmacol.* 2005;70:1861–1869.
36 Convertino M, Pellarin R, Catto M, Carotti A, Caflisch A. 9,10-Anthraquinone hinders beta-aggregation: how does a small molecule interfere with Abeta-peptide amyloid fibrillation? *Protein Sci.* 2009;18:792–800.
37 Yokoyama T, Ueda M, Ando Y, Mizuguchi M. Discovery of γ-mangostin as an amyloidogenesis inhibitor. *Sci Rep.* 2015;5:13570.
38 Huang K, Jiang L, Li H, Ye D, Zhou L. Development of anthraquinone analogues as phosphoglycerate mutase 1 inhibitors. *Molecules*. 2019;24:845.
39 Yokoyama T, Kosaka Y, Mizuguchi M. Crystal structures of human transthyretin complexed with glabridin. *J Med Chem.* 2014;57:1090–1096.
40 Yokoyama T, Kosaka Y, Mizuguchi M. Inhibitory activities of propolis and its promising component, caffeic acid phenethyl ester, against amyloidogenesis of human transthyretin. *J Med Chem.* 2014;57:8928–8935.
41 Pavelka K, Bruyère O, Cooper C, et al. Diacerein: Benefits, risks and place in the management of osteoarthritis. An opinion-based report from the ESCEO. *Drugs Aging.* 2016;33:75–85.
42 Zhang TJ, Li SY, Yuan WY, et al. Discovery and biological evaluation of some (1*H*–1,2,3-triazol-4-yl)methoxybenzaldehyde derivatives containing an anthraquinone moiety as potent xanthine oxidase inhibitors. *Bioorg Med Chem Lett.* 2017;27:729–732.
43 Zhang TJ, Li SY, Yuan WY, Zhang Y, Meng FH. Design, synthesis, and molecular docking studies of *N*-(9,10-anthraquinone-2-carbonyl)amino acid derivatives as xanthine oxidase inhibitors. *Chem Biol Drug Des.* 2018;91:893–901.
44 Bu X, Deady LW, Finlay GJ, Baguley BC, Denny WA. Synthesis and cytotoxic activity of 7-Oxo-7*H*-dibenz[f, i, j]isoquinoline and 7-Oxo-7H-benzo[e]perimidine derivatives. *J Med Chem.* 2001;44:2004–2014.
45 Mitter PC, Das-Gupta S, Bachhwat S. Anthraquinone series. *J Indian Chem Soc.* 1934;11:893–897.
46 Menendez CA, Nador F, Radivoy G, Gerbino DC. One-step synthesis of xanthones catalyzed by a highly efficient copper-based magnetically recoverable nanocatalyst. *Org Lett.* 2014;16:2846–2849.
47 Venkanna A, Goud PVK, Prasad PV, Shanker M, Rao PV. One-step synthesis of xanthones and thio-xanthones by using magnetically separable copper ferrite nanoparticles as a catalyst under ligand free conditions. *Chemistry Select.* 2016;1:2271–2276.
48 Baures PW, Oza VB, Peterson SA, Kelly JW. Synthesis and evaluation of inhibitors of transthyretin amyloid formation based on the non-steroidal anti-inflammatory drug, flufenamic acid. *Bioorg Med Chem.* 1999;7:1339–1347.
49 Adamski-Werner SL, Palaninathan SK, Sacchettini JC, Kelly JW. Diflunisal analogues stabilize the native state of transthyretin. Potent inhibition of amyloidogenesis. *J Med Chem.* 2004;47:355–374.
50 Bulawa CE, Connelly S, Devit M, et al. Tafamidis, a potent and selective transthyretin kinetic stabilizer that inhibits the amyloid cascade. *Proc Natl Acad Sci USA*. 2012;109:9629–9634.
51 Gales L, Macedo-Ribeiro S, Arsequell G, Valencia G, Saraiva MJ, Damas AM. Human transthyretin in complex with iododiflunisal: structural features associated with a potent amyloid inhibitor. *Biochem J.* 2005;388:615–621.
52 Razavi H, Palaninathan SK, Powers ET, et al. Benzoxazoles as transthyretin amyloid fibril inhibitors: synthesis, evaluation, and mechanism of action. *Angew Chem Int Ed Engl.* 2003;42:2758–2761.
53 Chen X, Murawski A, Patel K, Crespi CL, Balimane PV. A novel design of artificial membrane for improving the PAMPA model. *Pharm Res.* 2008;25:1511–1520.
54 Basak S, Mal D. Applications of [4+2] anionic annulation and carbonyl-ene reaction in the synthesis of anthraquinones, tetrahydroanthraquinones, and pyranonaphthoquinones. *J Org Chem.* 2017;82:11035–11051.
55 Elkazaz S, Jones PB. Photochemical hydroxylation of 1-methyl-9,10-anthraquinones: synthesis of 9'-hydroxyaloesaponarin II. *J OrgChem.* 2010;75:412–416.
56 Ruggli P, Brunner E. Anthracene derivatives. I. *o*-Nitroaldehydes of the anthraquinone series. *Helv Chim Acta.* 1925;8:155–168.
57 Quayle OR, Reid EE. Some substituted *o*-benzoylbenzoic acids and the corresponding anthraquinones. *J Am Chem Soc.* 1925;47:2357–2361.
58 Ashnagar A, Bruce JM. Synthesis of 2-bis(1-methylimidazol-2-yl)methoxycarbonyl-9,10-anthraquinone. *Int J Chem Tech Res.* 2011;3:1937–1940.
59 Leon JW, Whitten DG. Photodegradation of oligomeric polyesters containing anthraquinone and 1,2-diamine units. Single electron transfer induced cation radical bond cleavage in the solid state. *J Am Chem Soc.* 1995;117:2226–2235.
60 Witte PD, Lemli J. Synthesis of c-9-14C-1,8-dihydroxy-3-carboxyanthraquinone. *J. Labelled Compd Radiopharm.* 1998;25:23–33.
61 Williams AC, Camp N. Product class 4: benzopyranones and benzopyranthiones. *Sci Synth.* 2003;14:347–638.
62 Pan D, Wang Y, Li M, et al. Visible-light-induced aerobic oxidation of benzylic C(sp^3)-H of alkylarenes promoted by DDQ, *tert*-butyl nitrite, and acetic acid. *Synlett*. 2019;30:218–224.
63 Zhang X, Yang L, Wu Y, et al. Microwave-assisted transition-metal-free intramolecular Ullmann-type *O*-arylation in water for the synthesis of xanthones and azaxanthones. *Tetrahedron Lett.* 2014;55:4883–4887.
64 Eckstein M, Marona H. Preparation and properties of some 2-mercaptomethylxanthones. *Pol J Chem.* 1980;54:1281–1285.
65 Waszkielewicz AM, Gunia A, Szkaradek N, et al. Synthesis and evaluation of pharmacological properties of some new xanthone derivatives with piperazine moiety. *Bioorg Med Chem Lett.* 2013;23:4419–4423.
66 Zhang H, Shi R, Gan P, et al. Palladium-catalyzed oxidative double C-H functionalization/carbonylation for the synthesis of xanthones. *Angew Chem Int Ed.* 2012;51:5204–5207.
67 Rao H, Ma X, Liu Q, Li Z, Cao S, Li CJ. Metal-free oxidative coupling: Xanthone formation via direct annulation of 2-aryloxybenzaldehyde using tetrabutylammonium bromide as a promoter in aqueous medium. *Adv Synth Catal.* 2013;355:2191–2196.
68 Wang P, Rao H, Hua R, Li CJ. Rhodium-catalyzed xanthone formation from 2-aryloxybenzaldehydes via cross-dehydrogenative coupling (CDC). *Org Lett.* 2012;14:902–905.
69 Kottani R, Majjigapu JRR, Kurchan A, Majjigapu K, Gustafson TP, Kutateladze AG. Photoinduced signal amplification through controlled externally sensitized fragmentation in masked sensitizers. *J Am Chem Soc.* 2006;128:14794–14795.
70 Giri R, Goodell JR, Xing C, et al. Synthesis and cancer cell cytotoxicity of substituted xanthenes. *Bioorg Med Chem.* 2010;18:1456–1463.
71 Matsubara K, Mizuguchi M, Kawano K. Expression of a synthetic gene encoding human transthyretin in Escherichia coli. *Protein Expr Purif.* 2003;30:55–61.
72 Kabsch W. XDS. *Acta Crystallogr D Biol Crystallogr.* 2010;66:125–132.
73 Adams PD, Afonine PV, Bunkóczi G, et al. PHENIX: a comprehensive Python-based system for macromolecular structure solution. *Acta Crystallogr DBiol Crystallogr.* 2010;66:213–221.
74 Emsley P, Cowtan K. Coot: model-building tools for molecular graphics. *Acta Crystallogr D Biol Crystallogr.* 2004;60:2126–2132.
75 Sebaugh JL. Guidelines for accurate EC50/IC50 estimation. *Pharm Stat.* 2011;10:128–134.
76 Shah P, Kerns E, Nguyen DT, et al. An Automated high-throughput metabolic stability assay using an integrated high-resolution accurate mass method and automated data analysis software. *Drug Metab Dispos.* 2016;44:1653–1661.